CONTROL OF CASCADED THREE-LEVEL INVERTER FED INDUCTION MOTOR DRIVE USING HYBRID PWM METHOD

A Project Report

Submitted by

ALTHURTHI SAI BHARGAVA

in partial fulfilment of the requirement for the award

of the degree of

MASTER OF TECHNOLOGY

DEPARTMENT OF ELECTRICAL ENGINEERING

INDIAN INSTITUTE OF TECHNOLOGY MADRAS

CHENNAI-600 036, INDIA

JUN 2021

THESIS CERTIFICATE

This is to certify that the thesis titled **"CONTROL OF CASCADED THREE-LEVEL INVERTER FED INDUCTION MOTOR DRIVE USING HYBRID PWM METHOD"**, submitted by **A.SAI BHARGAVA**, to the Indian Institute of Technology, Madras, for the award of the degree of **Master of Technology**, is a bonafide record of the project work done by him under my supervision. The contents of this thesis, in full or in parts, have not been submitted to any other Institute or University for the award of any degree or diploma.

Prof. Srirama Srinivas

(Project Guide)

Dept. of Electrical Engineering

IIT-Madras, 600 036

Place : Chennai

Date :

ACKNOWLEDGEMENT

I would like to express my sincerest gratitude to Prof. Srirama Srinivas for giving me the opportunity to work on a project as ambitious as this one. The experiences I have gathered and the invaluable lessons I have learned while working on this project have endowed me with a renewed interest in the area of Power Electronic Converters and this would not have been possible without him guiding me every step of the way. Research would be a lot harder without well-meaning seniors to help skip a few hurdles. I would be forever grateful to Naga Suryaprakash for sharing with me his insights and experiences, pointing me to useful resources, helping me find new angles to look at the problem and above all, making the lab a much homelier place. I would like to thank my parents for always supporting me no matter what it is their support that gave me the assurance needed to pursue an M.Tech instead of doing a job. I have been truly blessed to have known all these people and I hope I can make it worthwhile for them as well through my work.

ABSTRACT

KEYWORDS: Cascaded inverter; three-level inverter; field oriented control: induction Motor; carrier-overlapped PWM; ripple content.

Multilevel inverters have emerged in a long way to become a part of industrial applications. Due to the inherent advantages achievable by the three-level inverters at lower switching frequencies, they are replacing the traditional two-level inverters in the low and medium power drives. A cascaded three-level inverter is a simple retrofit of two two-level inverters and is devoid of neutral point fluctuations, does not require any capacitor voltage initialisation and does not require more number of isolated dc sources when compared to its conventional counterparts like neutral point clamped (NPC), flying capacitor clamped (FCC) and cascaded H-bridge (CHB) types respectively. Pulse width modulation(PWM) schemes facilitate the generation of variable voltage at variable frequency at the output of the inverters for precise speed control in the motor drives. Most widely used PWM schemes in the motor drive applications are sinusoidal PWM, space vector PWM and selective harmonic PWM. Two carrier based PWM schemes are presented in this thesis to further improve the harmonic profiles of the above traditional PWM schemes.

The first part of this thesis presents the mathematical model of the induction motor and development of a closed loop Field-Oriented Control (FOC) for Induction Motor (IM) drive. FOC method is used for achieving a decoupled control of torque and flux for the IM drive. Rotor field orientation and indirect estimation of unit vector made the dynamic motor model and control logic further simple.

The second part of the thesis presents the advantages offered by the cascaded three-level inverter compared to the two-level inverter and a three-level NPC inverter firstly. Secondly, two carrier based PWM implementations namely Switching Frequency Optimal PWM (SFO-PWM) and Carrier Overlapped Switching Frequency Optimal PWM (CO-SFO-PWM) for the cascaded three-level inverter is presented. The offset introduced in the carrier signals in CO-SFO-PWM causes an overlap between them resulting in increased chopping of voltage wave at lower modulation indices and improving the motor current waveforms. However, it has reduced fundamental voltages at higher modulation indices. On the other hand, the SFO-PWM offers

higher fundamental voltage at these high modulation indices. It is observed from the results that incorporating CO-SFO-PWM at lower modulation indices and SFO-PWM at higher modulation indices is advantageous, instead of using a single PWM for entire modulation range. So, a hybrid PWM with a smooth switch over which combines the advantages of both the CO-SFO-PWM and SFO-PWM schemes is presented, which reduces overall ripple content in motor phase current for all the speed ranges. The output voltage and current harmonic profiles at lower and higher modulation indices are obtained and are closely compared with the conventional SPWM highlighting the merits and demerits of each PWM. Finally, the closed loop speed control of the induction motor drive using indirect rotor FOC with the proposed hybird PWM is simulated in MATLAB/SIMULINK and the performance of the drive highlighting the independent control of torque and flux for various dynamic speed and load changes are presented.

Contents

List of Figures

List of Tables

Chapter 1

Introduction

An electrical machine is heart of any drive system which facilitates bidirectional electro-mechanical energy transfer. This bidirectional conversion happens in a machine only when it is structured electrically, mechanically and thermally in a perfect way. The drive systems have many applications in various industrial mills, automobile propulsion, home appliances, transportation, computers and robotics etc., Among them industrial drive applications are generally classified into constant-speed and variable speed drives [1]. Previously, ac machines with constant frequency sinusoidal power supply have been used in constant-speed drive applications, whereas dc machines were preferred for variable speed drives. However, dc machines have the disadvantages of higher cost, higher rotor inertia and maintenance problems with commutator and brush arrangement which limits the speed and peak currents, causes electro-magnetic interference problems and do not permit it to operate in dirty and explosive environments whereas ac machines do not have these problems. An extensive research happened in variable frequency and variable speed ac machine drive technology over the last two or three decades reported in [1]-[3]. Although the dc drive converters and control is simple, progressively they are being replaced with ac drives due to their robustness.

The induction machine (IM) occupies a major hand in the present ac drive applications, particularly the cage type IM is most commonly used in industry due to its low cost and rugged construction. These machines are very reliable and available in fractional horse power (FHP) to multi-megawatt capacities. The low power FHP IMs are available in single-phase, but poly-phase

likely three-phase machines are used most often in variable speed drives.

1.1 Background

Usually, the most pronounced controlling methods of IM in literature [1] are Scalar control and Vector control. The scalar control technique involves the conventional open loop control methods like Voltage control, flux control, V/f control etc., Whereas in vector control i.e by the concept of Field Oriented Control (FOC) provides a closed loop control of IM with an independent control over flux and torque [1],[2]. Transforming the motor parameters into rotor frame of reference, decouples flux and torque of the machine [3].

Among different types of multilevel inverters available in literature [1],[8], the most widely used kinds are Neutral Point Clamped inverter (NPC), Flying Capacitor inverter (FCC) and Cascaded H-Bridge inverter (CHB) for modern medium and high power applications [8]. The NPC type has an easy control but it has neutral point voltage fluctuations. The FCC type require initialization and maintenance of voltage levels across capacitors. The CHB uses one separately isolated dc source for each H-bridge employed. Hence, a Dual two-level inverter i.e Cascaded three-level inverter offers a simple structure overcoming the above challenges mentioned for two-level and conventional thre-level inverters, and uses only two isolated dc sources for its operation.

PWM implementation in inverters provide variable output ac voltages at variable frequencies for a reliable speed control of IM. Revising about PWM techniques in literature [1],[12],[13], starting from most conventional SPWM to advanced SVPWM methods, each type has its own merits and demerits. Describing the conventional carrier and modulation wave based PWMs [11], modification of carrier waves improves output THD performance and modified modulating waves extends the linearity of output fundamental to overmodulation indices. For an improved overall performance, we require a hybrid PWM technique that captures the merits of the PWMs like Modified sine PWM (like SFO-PWM) and carrier ovelapped PWM (like CO-SFO-PWM).

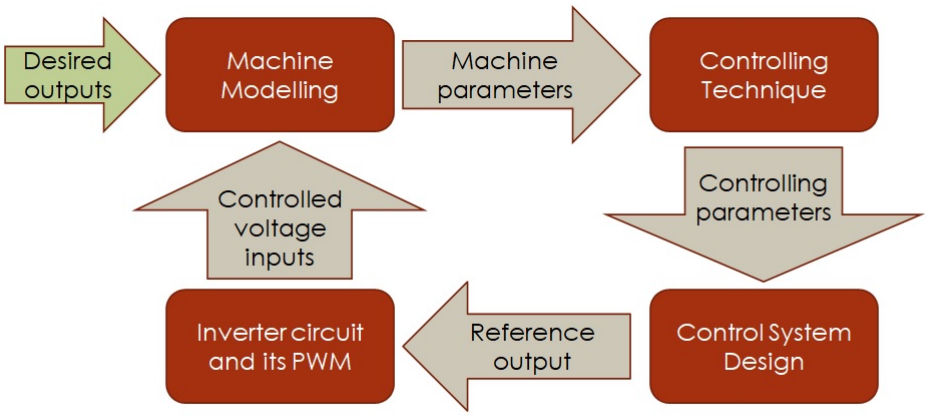

Fig. 1.1: Structure of project

1.2 Goals Of Project

The main objectives of the work reported in this thesis is,

- To devise a FOC controlled IM drive fed by a cascaded three-level inverter so as to achieve good torque dynamic performance.
- To devise carrier based PWM methods for the cascaded three-level inverter for reduced harmonic content in output phase currents.
- To devise a hybrid PWM transition method for wide range of rated speed operations of IM drive, without compromising the reliability and stability of control system.

1.3 Outline of the thesis

Sensationalizing and structuring the project work as shown in Fig. 1.1, each segment involves in various actions undergoing within the control system and has its own role to perform. The role and tasks of each of the above segments in Fig. 1.1 can be individually explained as follows,

Machine Model- This replicates the IM which is modelled with several blocks of transfer functions fed by input voltages and provides desired speed and torque outputs. Dynamic modeling of IM is the first step in designing this project.

Controlling Technique- By FOC method the control logic is developed, accordingly this block

includes the estimators of flux and electrical angle by following Indirect method of Rotor field orientation.

Control System Design- It covers the PI controllers adopted to produce stable and steady response of system quickly. This system in communication with estimators generate the values of voltages required in next step of change.

Inverter Circuit and its PWM- A dc powered cascaded three level inverter switched by Hybrid PWM technique comes under this segment. It generates the required output voltages from the reference modulating signals passed by the control system.

Provided all the above segments are being designed in a correct way and communicating well, the entire system will exhibit a reliable performance.

Depending on these functionalities of segments, the outline of thesis has been divided into the following chapters,

In Chapter 2 explanation of FOC method and designing the dynamic model of motor. The overall closed loop control under FOC method is developed as a simulate ready structure.

In Chapter 3 lists the most used inverter topologies in present power drive applications and explanation of their design. The study of conventional PWM techniques and their implementation is presented.

In Chapter 4 implementation of simulation model in MATLAB Simulink, discussion on the choice of inverter and PWM method that better fits for this application from the simulation results obtained. Incorporating this choice to the closed loop control model of IM and recording the observations describing motor performance.

In Chapter 5 a conclusion of entire work is noted.

Chapter 2

FOC Method for IM and Motor Model

The dynamic modelling of the system is the first essential thing to design a precise speed control mechanism. In an adjustable-speed drive, the machine normally constitutes an element within a feedback loop, and therefore its transient behaviour has to be taken into consideration. The dynamic performance of an IM is complex because three-phase rotor windings move w.r.t three-phase stator windings, which looks like a transformer with moving secondary where coefficient of coupling continuously varies with angular position. For such model, the dynamic derivations has differential equations with time varying mutual inductances which are complex to analyse. All these complexities are removed with the development of dynamic d-q model of motor as cited in [1],[3]. As a process, initially three-phase machine is represented by an equivalent two-phase machine in d-q axis and later this time varying d-q parameters are referred to an arbitrary reference frame where all time varying inductances are eliminated [1]. Hence, the final derived d-q model is simple for implementation. Besides, high-performance drive control like FOC require d-q model of the machine.

Induction motor control is classified as Scalar and vector control methods as reported in [1],[2]. In this, scalar control is simple to implement and have good steady state response but it has poor

dynamic response. But as modern day applications demand high dynamic response, FOC type has an increase of its prominence over past few decades. In FOC technique, the motor parameters are transformed to arbitrary rotating reference frame and it is aligned along the flux space vector of the machine (either rotor, stator or air-gap flux) and rotates at the speed of the flux vector. This transformation provides decoupling of the stator current components producing torque and flux, and hence allows an independent control over torque and flux of the IM. In fact, this advantage has made FOC method as a superior control technique for AC motor drives, similar to the control of separately excited DC machine where flux and torque current components are decoupled.

2.1 Field Oriented Control of IM

The fundamentals of vector control or Field-oriented control can be explained with the Fig. 2.1, where machine model is represented in synchronously rotating reference frame. In the Fig. 2.1, note that inverter is assumed with unity current gain and it is not represented here but say it generates i_a, i_b, i_c phase currents from the corresponding reference currents i_a*, i_b*, i_c* from the control system. Internally in the machine model shown in right of Fig. 2.1, a-b-c currents are converted into d-q currents in stationary reference frame and later converted to synchronously rotating frame with the help of electrical angle θ_e before getting applied to d-q model of machine. Following this, the controller is designed to have inverse transformation of these two stages and then the output references are given to the inverter. Within the process, unit vector of θ_e assures the correct alignment of i_{ds} current with flux vector and i_{qs} perpendicular to it as shown in Fig. 2.2. Collectively all the above computations happen instantaneously for producing responses to i_{ds} and i_{qs}.

Based on the generation of the unit vector, FOC can be either a direct method where θ_e is generated with phase vector flux signals from sensors or it can be indirect method where the θ_e is estimated from slip angle and slip frequency. Among them, Indirect method is easy to implement without adding any feedback loops and sensors to the control system.

In FOC method, the orientation of i_{ds} can be done along with either the rotor flux, the stator flux or the air-gap flux. But with rotor flux orientation as shown in Fig. 2.2, gives us

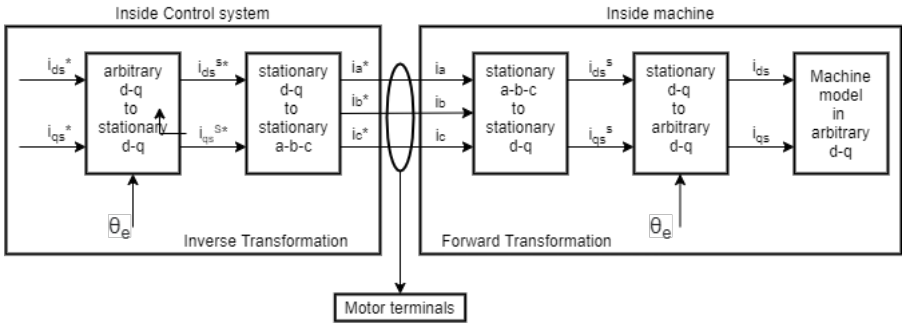

Fig. 2.1: Principle of FOC implementation

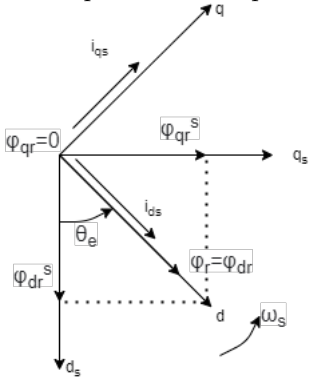

Figure 2.2: Phasor diagram for field vector orientation

natural decoupling control, where as other orientation options gives a coupling effect which has to be compensated by a decoupling compensation current, making unnecessary complication of the control logic. Hence, the Rotor field oriented indirect method of vector control provides us a simple and precise implementation, which is shown step by step in the following sections.

The dynamic model equations of Induction motor when referred to an arbitrary reference frame can be given as

$$\begin{bmatrix} V_{qs} \\ V_{ds} \\ V_{qr} \\ V_{dr} \end{bmatrix} = \begin{bmatrix} R_s + L_s\rho & \omega_s L_s & L_m\rho & \omega_s L_m \\ -\omega_s L_s & R_s + L_s\rho & -\omega_s L_m & L_m\rho \\ L_m\rho & (\omega_s - \omega_r)L_m & R_r + L_r\rho & (\omega_s - \omega_r)L_r \\ -(\omega_s - \omega_r)L_m & L_m\rho & -(\omega_s - \omega_r)L_r & R_r + L_r\rho \end{bmatrix} \begin{bmatrix} i_{qs} \\ i_{ds} \\ i_{qr} \\ i_{dr} \end{bmatrix} \tag{2.1}$$

in equation (2.1), V_{qs} and V_{ds} are direct and quadrature axis components of stator voltage, V_{qr} and V_{dr} are direct and quadrature axis components of rotor voltage, i_{qs}, i_{ds}, i_{qr}, i_{dr} are corresponding current components,ϕ_{qs}, ϕ_{ds}, ϕ_{qr}, ϕ_{dr} are corresponding flux components, R_s is Stator winding resistance per phase, L_s is Stator winding Inductance per phase, R_r, L_r are corresponding rotor

parameters, L_m is Mutual inductance between stator and rotor windings, ω_s is Synchronous speed of motor in electrical radians, ω_r is Rotor speed in electrical radians respectively.

Considering the torque equation of motor from the dynamic model can be given as

$$T = \frac{P}{2}\frac{L_m}{L_r}(i_{qs}\phi_{dr} - i_{ds}\phi_{qr}) \tag{2.2}$$

As the rotor windings are being shorted, then

$$i_{qr} = \frac{\phi_{qr} - L_m i_{qs}}{L_r} \tag{2.3}$$

$$i_{dr} = \frac{\phi_{dr} - L_m i_{ds}}{L_r} \tag{2.4}$$

$$V_{qr} = 0; V_{dr} = 0 \tag{2.5}$$

Then the equation set of (2.1) gets modified as follows

$$\begin{bmatrix} V_{qs} \\ V_{ds} \\ 0 \\ 0 \end{bmatrix} = \begin{bmatrix} R_s + L_s\sigma\rho & \omega_s L_s\sigma & \frac{L_m}{L_r}\rho & \omega_s\frac{L_m}{L_r} \\ -\omega_s L_s\sigma & R_s + L_s\sigma\rho & -\omega_s\frac{L_m}{L_r} & \frac{L_m}{L_r}\rho \\ -\frac{R_r}{L_r}L_m & 0 & \frac{R_r}{L_r} + \rho & (\omega_s - \omega_r) \\ 0 & -\frac{R_r}{L_r}L_m & -(\omega_s - \omega_r) & \frac{R_r}{L_r} + \rho \end{bmatrix} \begin{bmatrix} i_{qs} \\ i_{ds} \\ \phi_{qr} \\ \phi_{dr} \end{bmatrix} \tag{2.6}$$

Modifying the equation set (2.6), we have

$$V_{qs} = (R_s + \sigma L_s\rho)i_{qs} + [\omega_s\sigma L_s i_{ds} + \omega_s\frac{L_m}{L_r}\phi_{dr}] \tag{2.7}$$

$$V_{ds} = (R_s + \sigma L_s\rho)i_{ds} + [-\omega_s\sigma L_s i_{qs} + \frac{L_m}{L_r}\rho\phi_{dr}] \tag{2.8}$$

$$\phi_{dr} = \frac{1}{\omega_s - \omega_r}\frac{R_r}{L_r}L_m i_{qs} \tag{2.9}$$

$$0 = -\frac{R_r}{L_r}L_m i_{ds} + \frac{R_r}{L_r}\phi_{dr} + \rho\phi_{dr} \tag{2.10}$$

and the Torque equation (2.2) gets modified as,

$$T = \frac{P}{2}\frac{L_m}{L_r}i_{qs}\phi_{dr} \tag{2.11}$$

Let us say, $E_q = [\omega_s\sigma L_s i_{ds} + \omega_s\frac{L_m}{L_r}\ \phi_{dr}]$ and $E_d = [-\omega_s\sigma L_s i_{qs} + \frac{L_m}{L_r}\rho\phi_{dr}]$ as two emf terms

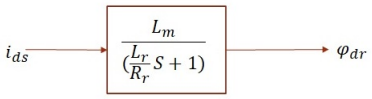

Fig. 2.3: Estimation of Flux

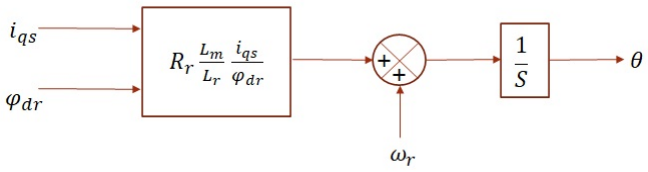

Fig. 2.4: Estimation of Electrical angle

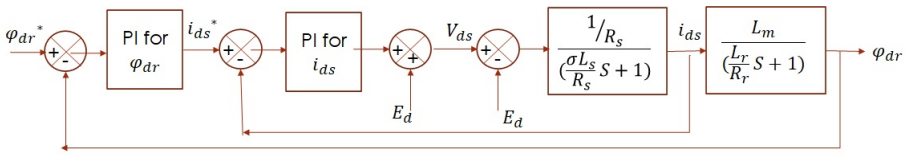

Fig. 2.5: Decoupled d-axis current loop

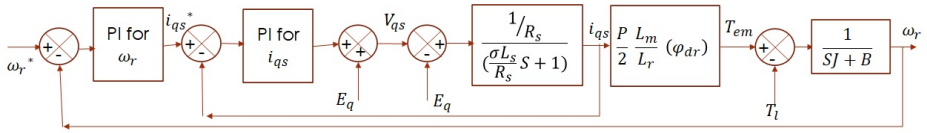

Fig. 2.6: Decoupled q-axis current loop

in equations (2.7) and (2.8) which helps in obtaining a first order relation between voltage and current along d and q axis independently.

By this Indirect vector control, from equation (2.10) the rotor flux is estimated as shown in Fig. 2.3 and from equation (2.9) electrical angle is estimated as shown in Fig. 2.4.

Reconsidering the emf terms, E_d and E_q are set as feed-forward terms and are added to V_{ds} and V_{qs} as shown in Fig. 2.5 and Fig. 2.6. As a result the d-axis and q-axis control loops got decoupled and formed into two isolated loops, it is the step where we are enabled with independent controlling of Flux and Torque.

2.1.1 Calculation of rated parameters

Consider the Table 2.1 showing the specifications of motor model that is used in this project. From general torque and power relation, rated torque can be expressed as

Table 2.1: Motor Specifications

SPECIFICATION	VALUE
Power (P)	4000 W
Voltage (v)	400 V
Frequency (f)	50 Hz
Number of poles (P)	4
Rated speed (N)	1430 rpm
Stator Resistance (R_s)	1.405 Ω
Rotor Resistance (R_r)	1.395 Ω
Stator Inductance (L_s)	0.178 H
Rotor Inductance (L_r)	0.178 H
Mutual Inductance (L_m)	0.1722 H
Friction coefficient (B)	0.002985 Nm-sec
Inertia constant (J)	0.0131 Kg-m^2

$$T_{rated} = \frac{P_{rated}}{\omega_{r_{rated}}} \tag{2.12}$$

Rearranging equation (2.9), we have

$$i_{qs} = \frac{(\omega_s - \omega_r) * \phi_r * L_r}{L_m * R_r} \tag{2.13}$$

Substituting above equation (2.13) in (2.11), we can derive

$$\phi_r = \sqrt{\frac{T * R_r}{(\omega_s - \omega_r) * 0.5 * P}} \tag{2.14}$$

Forming steady state equations of (2.10), (2.8) and (2.7) respectively, we have

$$i_{ds} = \frac{\phi_r}{L_m} \tag{2.15}$$

Table 2.2: Rated value of parameters

PARAMETER	RATED VALUE
Load Torque (T)	26.7113 Nm
Voltage (v)	400 V
Rotor field flux (ϕ_r)	1.1273 Wb
Stator q-axis current (i_{qs})	12.2491 A
Stator d-axis current (i_{ds})	6.5465 A
Stator q-axis Voltage (V_{qs})	383.3721 V
Stator d-axis Voltage (V_{ds})	-35.0044 V

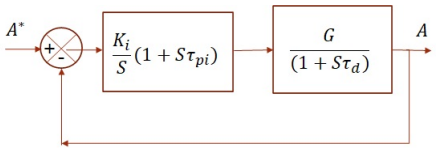

Fig. 2.7: Sample PI controller loop

$$V_{ds} = R_s i_{ds} - L_s \sigma \omega_s i_{qs} \tag{2.16}$$

$$V_{qs} = R_s i_{qs} - L_s \sigma \omega_s i_{ds} + \frac{L_m}{L_r} \omega_s \phi_r \tag{2.17}$$

Substituting the motor specification values in above derivations, we can calculate the rated parameter values as in Table 2.2.

2.2 Calculation of gain constants for PI controllers

Consider a sample first order transfer function system with a PI controller as shown in Fig. 2.7. Let K_p and K_i are proportional and integral constants of PI controller, τ_{pi} and τ_d are time constants of PI controller and first order system, G be the gain of first order system respectively. Then, $\tau_{pi} = \frac{K_p}{K_i}$. By implementing pole-zero cancellation, we get

$$\tau_{pi} = \tau_d \tag{2.18}$$

Table 2.3: PI controller gain constant values

PI CONTROLLER LOOP POSITION	K_p VALUE	K_i VALUE
Current Loops	1.405	171.856
Rotor Flux Loop	5.8072	45.5015
Rotor Speed Loop	0.003	0.00068

and for unity loop gain,

$$K_p * G = 1 \tag{2.19}$$

using the above two conditions shown in equation (2.18) and (2.19), for each individual closed loop in Fig.s 2.5 and 2.6 we can derive for gain constants.

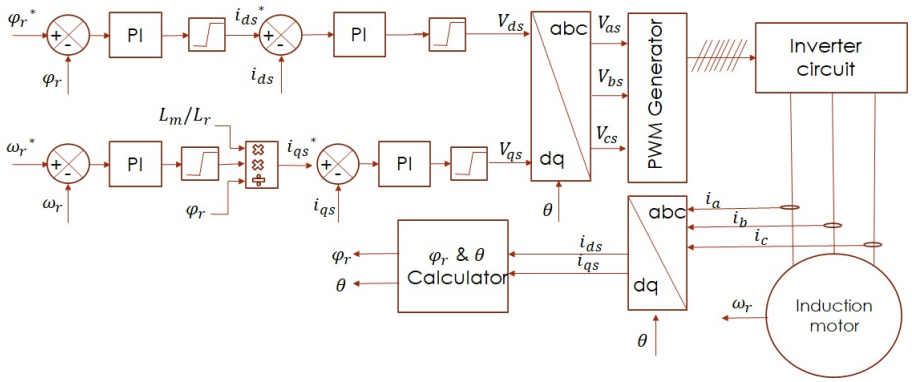

Fig. 2.8: Block diagram of Rotor-field oriented FOC control technique

As both the current loops are identical, gain constants are same for both the loops. If K_{pi} and K_{ii} are proportional and integral gain constants for current loops, then

$$K_{pi} = R_s \tag{2.20}$$

$$K_{ii} = \frac{R_s^2}{\sigma L_s} \tag{2.21}$$

similarly for Flux loop, if $K_{p\phi}$ and $K_{i\phi}$ are respective gain constants, then

$$K_{p\phi} = \frac{1}{L_m} \tag{2.22}$$

$$K_{i\phi} = \frac{R_r}{L_m L_r} \tag{2.23}$$

and for Speed loop, if $K_{p\omega}$ and $K_{i\omega}$ are respective gain constants, then

$$K_{p\omega} = B \tag{2.24}$$

$$K_{i\omega} = \frac{B^2}{J} \tag{2.25}$$

after substitution of values, the calculated K_p and K_i are tabulated in Table 2.3. These values will be further tuned while simulating in MATLAB.

Taking all the points in this chapter into consideration, the final block diagram for our Rotor-flux oriented FOC method is shown in Fig. 2.8. In this, the inverter circuit and PWM blocks shall be discussed in upcoming chapters.

Chapter 3

Power Inverters and PWM Techniques

An inverter circuit of any motor drive works like a controllable nozzle between DC power source and terminal motor. It consists of power semiconductor switches which are triggered cyclically in a sequence and converts the power from the DC sources into a controllable AC output power with variable voltage and frequency. Depending on the harmonic performance and number of levels of output voltage generated by the inverters, a wide variety of multi level inverter topologies are reported in the literature [8],[9]. Among them the most popular topologies are Neutral point clamped type (NPC), Flying capacitor type(FCC), Cascaded H-Bridge type (CHB) and Cascaded Three-Level Inverter. More the number of voltage levels provides better AC output with reduced distortions, but as voltage levels increase both complexity and cost also increases. Each topology of the multi level invetrer has its own advantages and disadvanatges. A simple two-level inverter is more suitable in a low cost and low power application, while for medium power levels, NPC, FCC and Cascaded thee-level are more suitable [9]. However, the NPC converter suffers from the neutral point fluctuation problems while in the FCC topology, owing to the use of large number of capacitors, the charge balancing and the voltage initialization are very difficult. On the other hand, a CHB inverter demands more number of isolated dc sources. The three level Cascaded

inverter does not require any clamping diodes as in other three level NPC or FCC topology and it requires only two isolated dc sources when compared to three in a three-level CHB. The capacitors in the cascaded inverter only carry the dc ripple current and hence it is free form neutral point fluctuations which are predominant in the NPC topology. Owing to these advantages, in the present work, the cascaded-three level inverter is chosen. The improvement in the performance characteristics obtained with the cascaed inverter compared to a conventional two-level inverter and three level NPC converter are presented in chapter 4.

Pulse Width Modulation (PWM) technique enables the power inverter to generate the required voltage for the speed control of motor drives. The type of PWM technique determines the output power quality and control of a power inverter. For any PWM technique, commonly desired outcomes are a low harmonic distortion of outputs, linear voltage control w.r.t changing speed and less ripple content. The PWM methods reported in the literature [1],[12],[15] can be broadly classified as SVPWM based and carrier based depending on the type of implementation. The SVPWM method is based on the volt second balance of the required voltage vector with the nearest three voltage vectors generated by the inverter, while the carrier based methods involve comparison of a sinusoidal modulating waveform at required frequency with a high frequency carrier waveform. Some of the carrier based methods that are reported in the literature [10],[11] are, Sinusoidal-PWM (SPWM), Switching Frequency Optimal PWM (SFO-PWM), Carrier Overlapped sine PWM (CO-SPWM), CO-SFO-PWM and many other hybrid PWMs. Each of these PWMs can be implemented for any multilevel inverter simply with (n-1) carriers where each carrier wave is adhered to one pair of switching rows. The (n-1) carrier waves can be generated in different ways like Alternative Phase Opposition (APO), Phase Opposition (PO), Phase Disposition (PD) and PO-PD are discussed in [21]. Among them, the PD scheme results in a better harmonic performance reported in [21] and hence this is used for the present work.

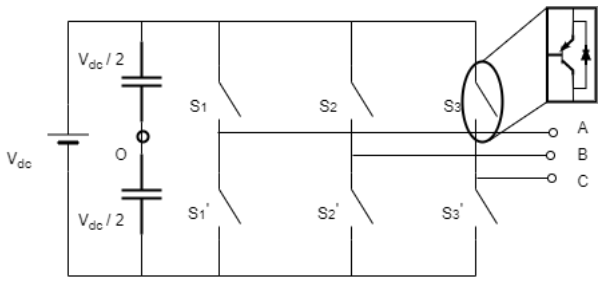

Fig. 3.1: Two-level inverter circuit

Table 3.1: Switching combinations for two-level inverter

S1	S1'	V_{Ao}
1	0	$+V_{dc}/2$
0	1	$-V_{dc}/2$

3.1 Inverter Circuits

3.1.1 Two-Level Inverter

A basic two level inverter circuit has six power switches (two switches at each phase leg) connected and each switch is realised with an IGBT with an anti parallel body diode as shown in Fig. 3.1. This inverter is capable of generating a two-level pole voltage at its output. The level of the output pole voltage V_{Ao} along with the status of the switches in a-phase leg of the inverter is shown in Table 3.1. The bottom switches S1', S2', S3' always exhibit complimentary switching for S1, S2, S3 respectively.

3.1.2 Three-Level Neutral Point Clamped Inverter

A three-level NPC inverter circuit has Twelve power switches (Four switches per each phase leg) connected and six power diodes for facilitating Neutral point clamping, as shown in Fig. 3.2. This inverter can provide three voltage levels at each pole i.e $+V_{dc}/2$, 0 and $-V_{dc}/2$ corresponding to the switching Table 3.2. Within the four rows of switches, the first two rows i.e (S1,S2,S3) and (S1',S2',S3') are complementary pair and the next two rows i.e (S4,S5,S6) and (S4',S5',S6') are complementary pairs respectively.

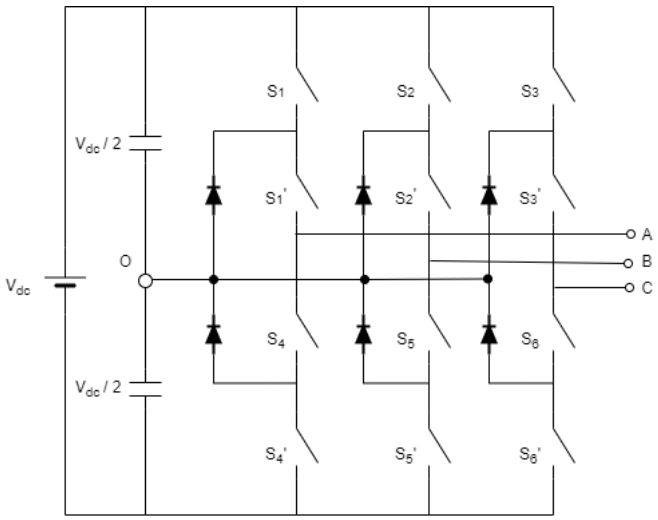

Fig. 3.2: Three-level NPC inverter circuit

Table 3.2: Switching combinations for Three-level NPC inverter

S1	S1'	S4	S4'	V_{Ao}
1	0	1	0	$+V_{dc}/2$
0	1	1	0	0
1	0	0	1	$-V_{dc}/2$

3.1.3 Cascaded Three-Level Inverter

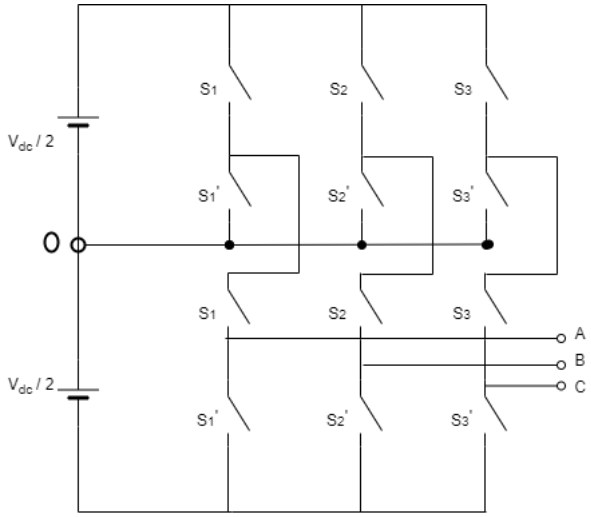

Fig. 3.3: Three-level cascaded inverter circuit

The Cascaded Three-Level inverter circuit can be realized as simple cascaded connection of two Two-Level inverters which make the circuit free from neutral point fluctuations. Like other three

Table 3.3: Switching combinations for cascaded three-level inverter

S1	S1'	S4	S4'	V_{Ao}
0	1	0	1	-$V_{dc}/2$
0	1	1	0	0
1	0	1	0	+$V_{dc}/2$

level inverter, this circuit also has twelve power switches (Four switches at each phase leg), as shown in Fig. 3.3. This inverter can provide three voltage levels at each pole i.e 0, $V_{dc}/2$ and V_{dc} corresponding to the switching Table 3.3. The switching complimentary are same like NPC type.

A detailed comparison of the outputs of the above discussed topologies for a sinusoidal PWM control are presented in chapter 4.

3.2 PWM Techniques

In this section, various carrier based pwm methods like sinusoidal PWM, SFO-PWM and CO-SFO-PWM for the cascaded three level inverter are discussed. For the three-phase three-level inverter PWMs, three modulation waves each being 120 degrees phase displaced and two carrier signals are used for pulse generation. The carrier reference for top switches has its mean axis in positive half plane while that of bottom switches carrier occupy negative half plane as shown in Fig. 3.4. At any instant, the PWM switching decides the pole voltage V_{Ao} of cascaded three-level inverter as

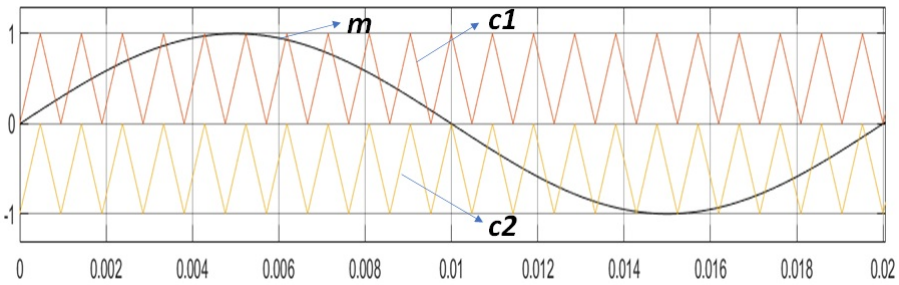

Fig. 3.4: Example of SPWM implementation

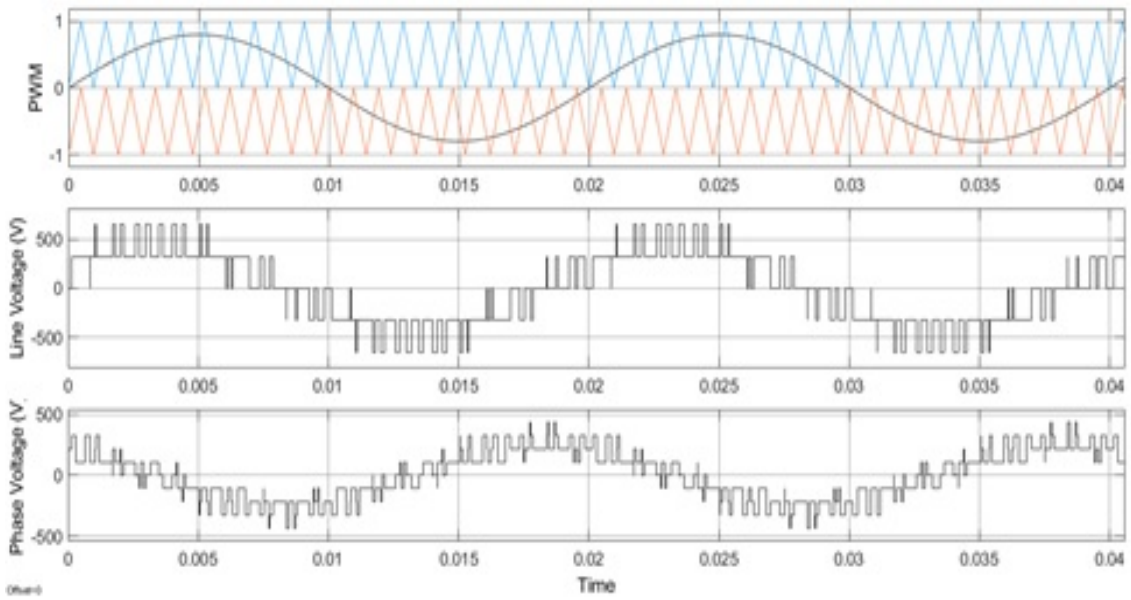

Fig. 3.5: PWM, Line voltage, Phase voltage waveforms for SPWM at m_a=0.8

$$\begin{aligned} \mathbf{V}_{Ao} &= +V_{dc}/2 \quad ; for(m > c1) and (m > c2) \\ \mathbf{V}_{Ao} &= 0 \qquad\quad ; for(m < c1) and (m > c2) \\ \mathbf{V}_{Ao} &= -V_{dc}/2 \quad ; for(m < c1) and (m < c2) \end{aligned} \tag{3.1}$$

while, V_{dc} is the DC source voltage, m is instantaneous value of A-phase reference modulation wave, c1, c2 are instantaneous values of carrier reference for Top and bottom switches respectively.

The polarity of output voltage at an instant is decided by equations in (3.1). But, the magnitude of output voltage is decided by the following logic.

$$m_a = \frac{A_m}{(n-1) * A_c} \tag{3.2}$$

$$m_f = \frac{f_c}{f_m} \tag{3.3}$$

while, m_a is amplitude modulation Index, m_f is frequency modulation Index, A_m and A_c are Peak to Peak amplitudes of modulation and carrier waves, f_m and f_c are frequencies of modulation and carrier waves, n being number of levels of Inverter respectively.

3.2.1 Sinusoidal Pulse Width Modulation

A sinusoidal PWM method is most basic technique where modulating sine wave is compared with level shifted triangular carrier signals as shown in Fig. 3.5.

For a SPWM implemented three-level inverter, $V_{dc}/2$ is the maximum peak that can be seen for a phase voltage output of inverter. Hence, for a V_{ph-rms} fundamental rms output phase voltage

$$V_{dc}/2 = \sqrt{2} * V_{ph-rms} \tag{3.4}$$

then, $V_{L-L-rms}$ rms line to line fundamental rms voltage can be given as

$$V_{L-L-rms} = \sqrt{3/2} * \frac{V_{dc}}{2} \tag{3.5}$$

So, to get 400v Line-Line rms value of fundamental at unity m_a, we require 650v of V_{dc} as per equation (3.5). With a 650v input DC and m_a=0.8, m_f=21, SPWM is implemented and the output voltage responses are shown in Fig. 3.5, the line voltage has five levels and the phase voltage has nine voltage levels in their output. The phase voltage seems to be more near to sinusoidal.

3.2.2 Switching Frequency Optimal-PWM

In SFO-PWM, the modified sinusoidal wave is used as modulating wave but the carriers are held same like SPWM. The modified sine wave is generated by addition of offset voltage signal as shown in Fig. 3.6, which can be derived as shown below,

$$v_o = -(\frac{max(v_a, v_b, v_c) + min(v_a, v_b, v_c)}{2}) \tag{3.6}$$

$$\begin{aligned} v_{am} &= v_a + v_o \\ v_{bm} &= v_b + v_o \\ v_{cm} &= v_c + v_o \end{aligned} \tag{3.7}$$

While, v_a, v_b, v_c are the modulating sine waves for a three phases, v_{am}, v_{bm}, v_{cm} are modified modulating waves for three phases, v_o being the offset voltage respectively.

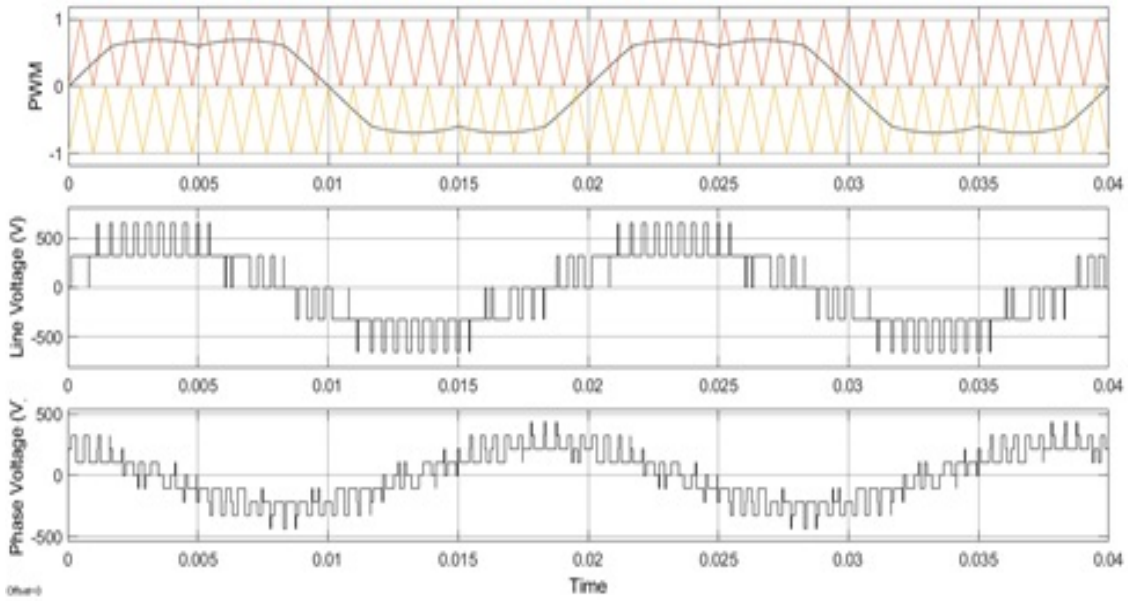

Fig. 3.6: PWM, Line voltage, Phase voltage waveforms for SFO-PWM at m_a=0.8

Except the generation of modulating wave, rest other parameters are followed same as SPWM and the results are shown in Fig. 3.6. Like SPWM, the SFO-PWM also has the phase voltage more near to sinusoidal with same nine levels in output.

3.2.3 Carrier overlapped-SFO-PWM

In Carrier overlapped-PWM, modified carrier waves are generated by addition of an injected voltage v_{inj} [11]. Mostly, in CO-PWM an additional magnitude of 0.5 is extended at upper and lower limits for a unity magnitude triangular carrier as shown in figure 3.6. For CO-SFO-PWM, this carrier overlapping is implemented for SFO-PWM provided with the same parameters followed previously except that the carriers are being modified. From the recorded responses shown in Fig. 3.7, the voltage levels are same as SFO-PWM. The Carrier overlapped method generates a 50 percent overlap area between two carrier waves facilitating to double the m_f at lower modulation indices. As a result, this doubled m_f greatly impacts on reducing the THD values at this lower m_a.

The CO-SFO-PWM is highly beneficiary in reducing THDs for lower modulation index oper-

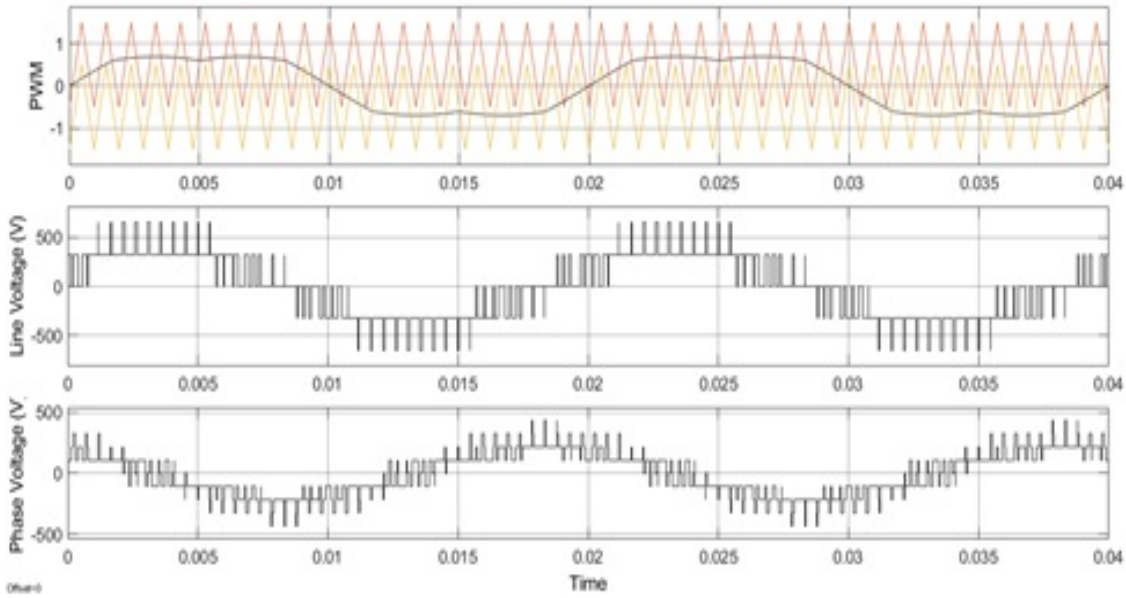

Fig. 3.7: PWM, Line voltage, Phase voltage waveforms for CO-SFO-PWM at m_a=0.8

ation of motor drive but it has to be switched over to noncarrier overlap PWM like SFO-PWM at higher modulation indices for reaping maximum benefits in overall modulation range, which is presented in the reference [10]. Instead of sudden switchover from CO-SFO-PWM to SFO-PWM mentioned in [10], a hybrid PWM technique which provides a soft transition between these PWMs is simulated and explained in following subsection 4.2.1.

Chapter 4

Results and Discussion

The proposed FOC with hybrid PWM for the induction motor drive is simulated in MATLAB and the results are presented in detail. Firstly, open loop v/f results with conventional SPWM on the three-level cascaded inverter circuit are compared to that of a conventional three-level NPC and a two-level inverter highlighting the merits of the cascaded inverter. Secondly, the three PWM methods discussed in chapter 3 namely SPWM, SFO PWM and CO-SFO PWM and the proposed hybrid PWM are simulated on the three-level cascaded inverter with a RL load of (10kW, 1kVAr, 400V) for the full range of modulation index form 0 to 1 are presented to showcase the advantages of the hybird PWM. Finally FOC with the proposed hybrid PWM on the cascaded three-level inverter fed induction motor drive is simulated and the dynamic and steady state results obtained are presented in detail in this chapter. The dc link voltage is taken as 650V for all the simulations and the value of the frequency modulation index mf is maintained at 21 for all the simulations for a fair comparison. A discreet time fixed step solver is used in MATLAB for all the simulations. The motor parameters and the induction motor parameters are given in detail in chapter 2 of this report. The data for five fundamental cycles and the harmonic content till 63^{rd} harmonic is taken in all the FFT analysis plots for the calculation of the voltage and current THD.

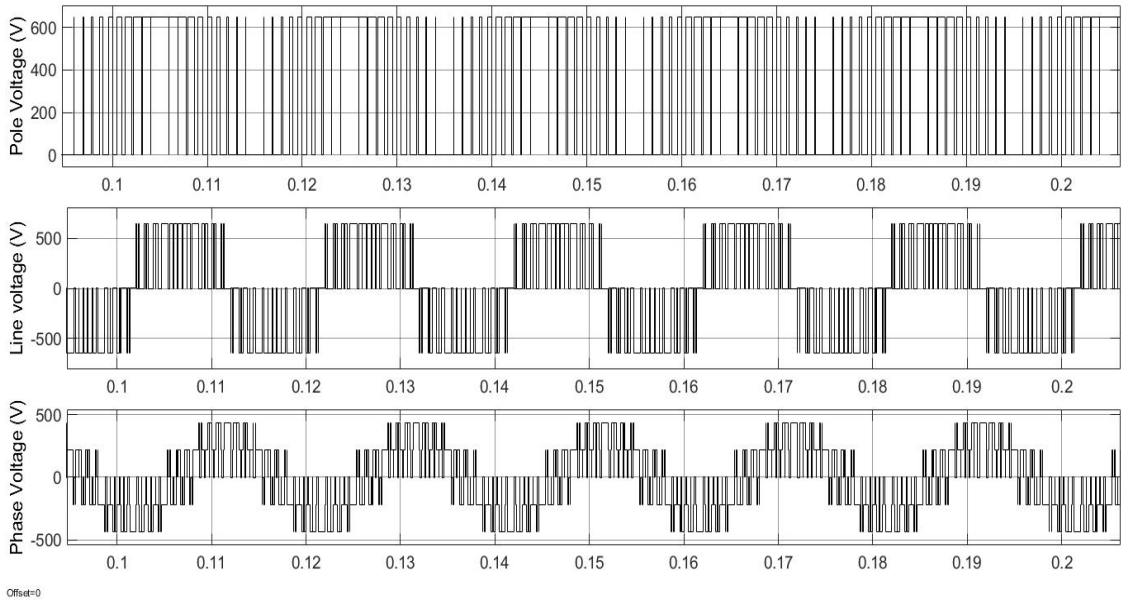

(a) Voltage waveforms

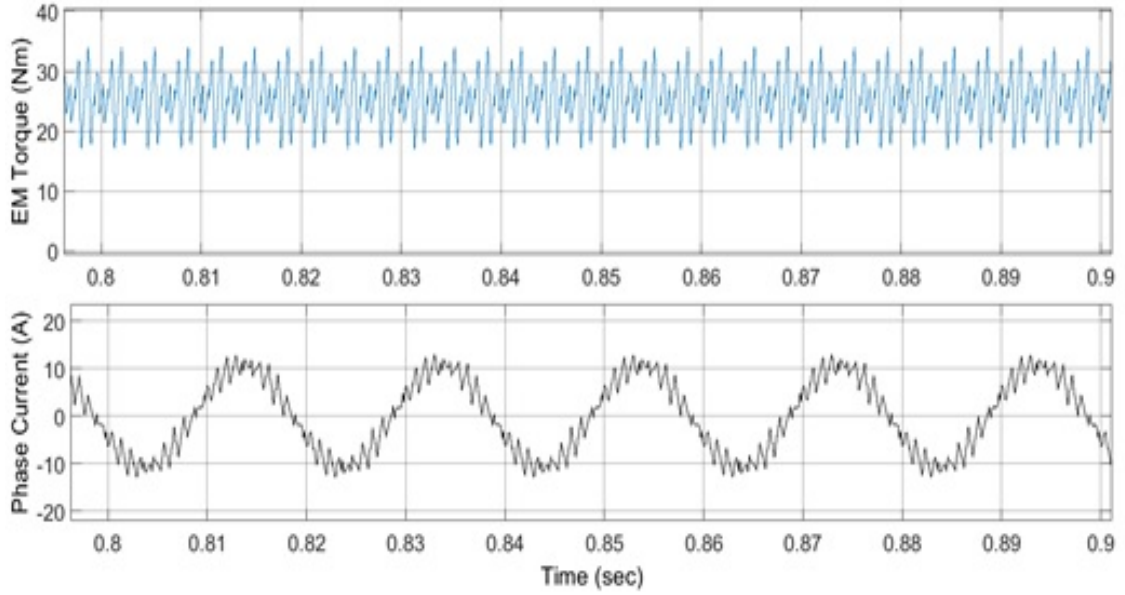

(b) Torque and Current response

Fig. 4.1: Simulation results of the Two level inverter fed induction motor drive in open loop with conventional SPWM

4.1 Open loop V/f results of two-level and three-level inverter fed induction motor drive

The steady state results obtained at the rated speed with open loop v/f control showing the speed and torque along with the pole, line and phase voltages for the induction motor drive fed from

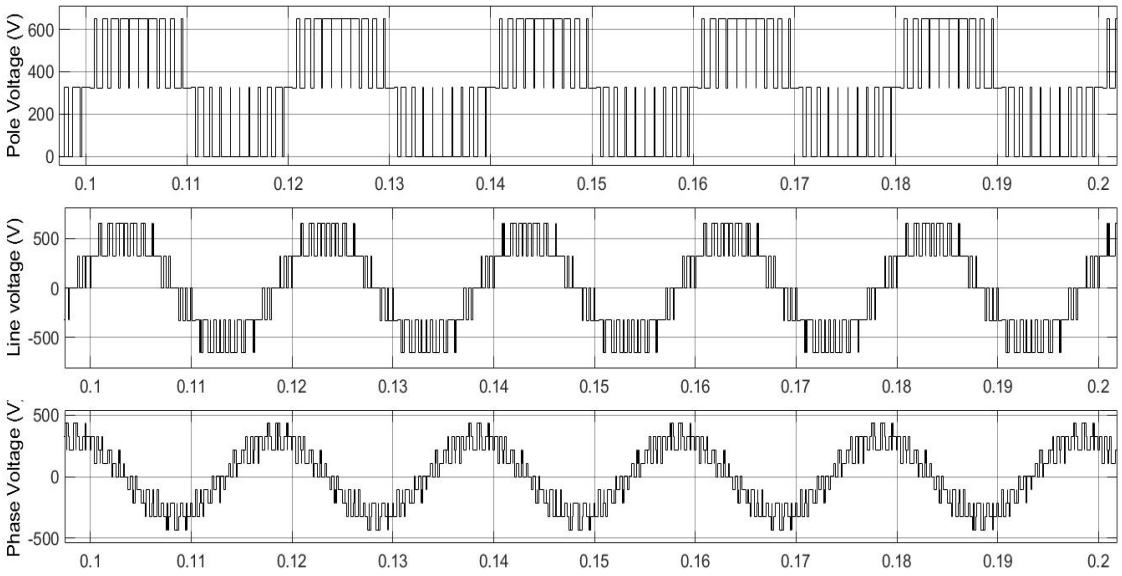

(a) Voltage waveforms

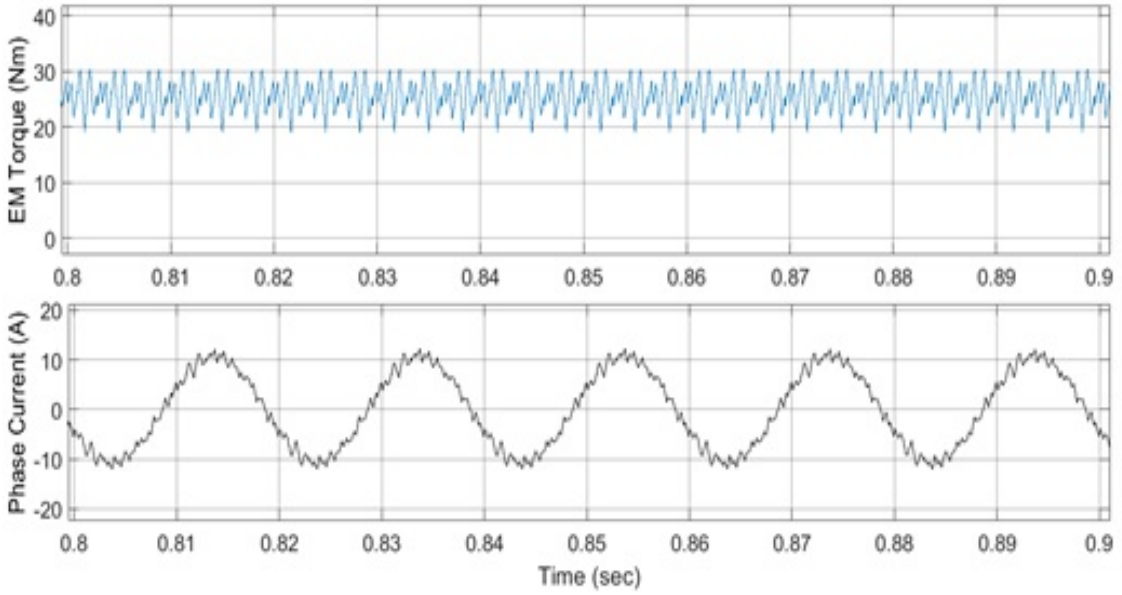

(b) Torque and Current response

Fig. 4.2: Simulation results of the Three-level NPC inverter fed induction motor drive in open loop with conventional SPWM

two-level inverter, three level NPC inverter and the three-level cascaded inverter are shown in Figs. 4.1 - 4.3 respectively.

It can be observed from the voltage waveforms presented in Figs. 4.1 - 4.3 that the output

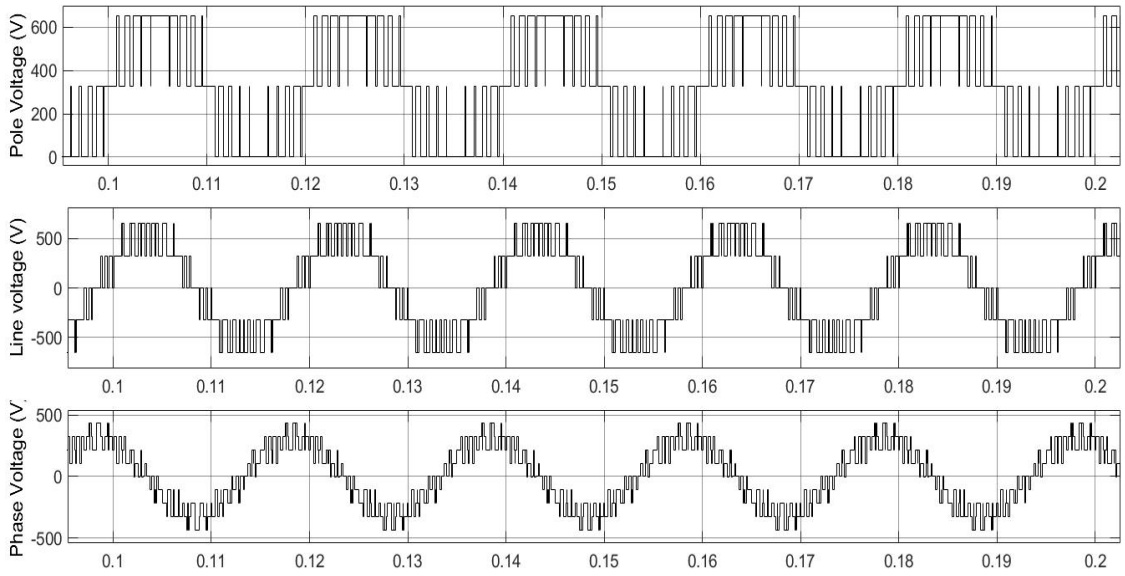

(a) Voltage waveforms

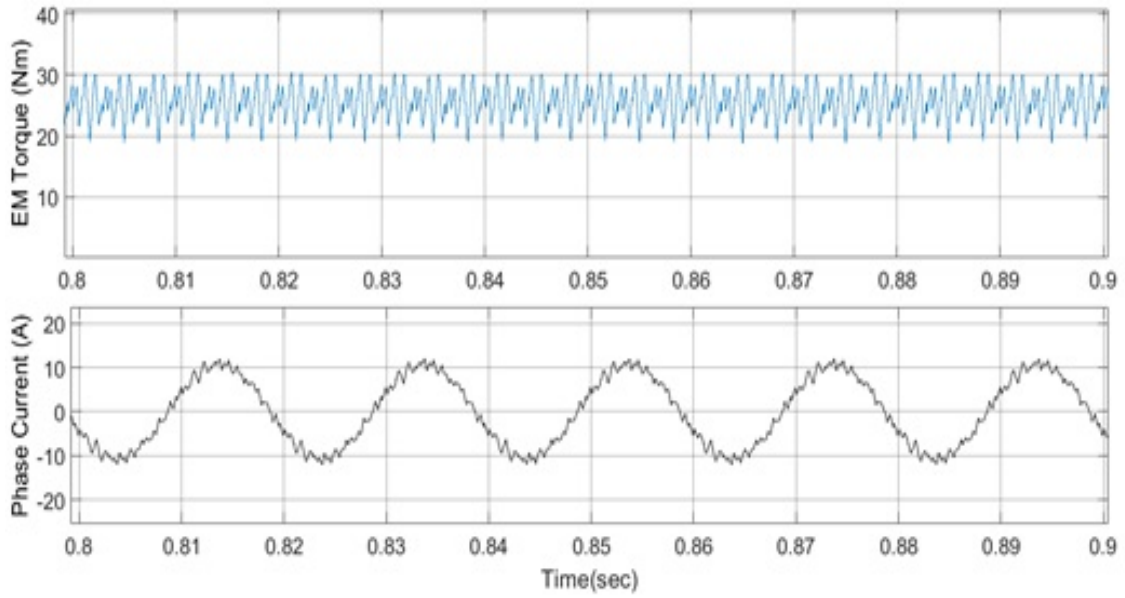

(b) Torque and Current response

Fig. 4.3: Simulation results of the Three-level cascaded inverter fed induction motor drive in open loop with conventional SPWM

phase voltage with the three level inverters is more closer to a pure sine wave having nine levels when compared to the five levels in the two level inverter. From the Figs. 4.1(b), 4.2(b) and 4.3(b), the torque ripple obtained with the three level inverters is 32% and the torque ripple obtained

with the two-level inverters is 45%. It can be clearly seen that the torque ripple is considerably reduced with the use of three level inverter. The torque and current response with the cascaded inverter is almost the same with that of the three-level NPC however, the cascaded inverter does not suffer form neutral point fluctuations and hence is chosen in the present work.

4.2 Simulation of PWMs on cascaded three-level inverter with RL load

The PWM methods discussed in the previous chapter, SPWM, SFO PWM and CO-SFO-PWM are implemented on the cascaded inverter connected to a three phase RL load (10KW,1KVAR,400V) and the performance of them in terms of the voltage THD and current THD for the modulation index of 0.3, 0.8, 1.2 are shown in Figs. 4.4 -4.6. For all the simulation results, PD method of carrier wave generation is followed and V/f ratio of modulation wave is maintained. The fundamental frequency at unity m_a being equal to 50Hz. The frequency modulation factor m_f is set equal to 21, allowing the carrier wave frequency to vary along with fundamental frequency as m_a varies.

Firstly, comparing THD responses of three PWMs, it can be observed from the results shown in Figs. 4.4(d), 4.5(d) and 4.6(d), the CO-SFO-PWM has good reduction in harmonic magnitudes especially the lower orders. Also the THD in the phase current at lower modulations is considerably less with the CO-SFO-PWM, which can be inferred from Figs. 4.4(g), 4.5(g) and 4.6(g). However, at higher modulation and overmodulation ranges, the THDs are almost approaching same values for all the methods. Because of doubling of m_f happened due to carrier overlapping method, in carrier overlap region the modulation wave encounters more number of carrier crossings than usual carrier method, and hence produces more number of voltage pulses ultimately increasing harmonic order and reduction of THD. The increased number of pulses and less distorted current output for CO-SFO-PWM at m_a=0.3 can be clearly observed among Figs. 4.4(a), 4.5(a) and 4.6(a) and thus in the lower modulation index range, CO-SFO-PWM is beneficial over the other two PWMs.

Further, it can be seen from the Figs. 4.4(d), 4.5(d) and 4.6(d), all the three PWM methods

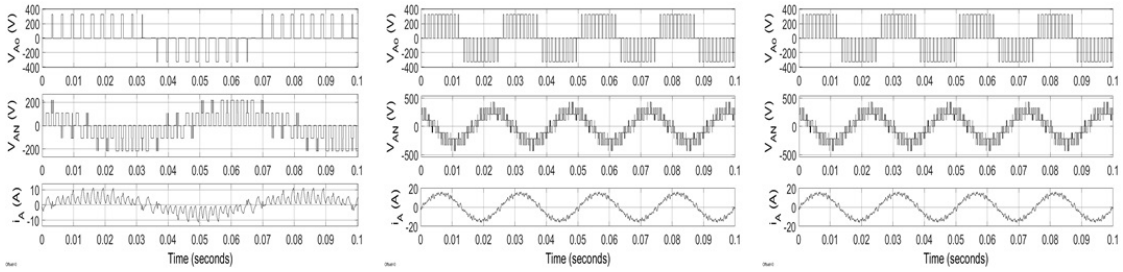

(a) For m_a=0.3 (b) For m_a=0.8 (c) For m_a=1.2

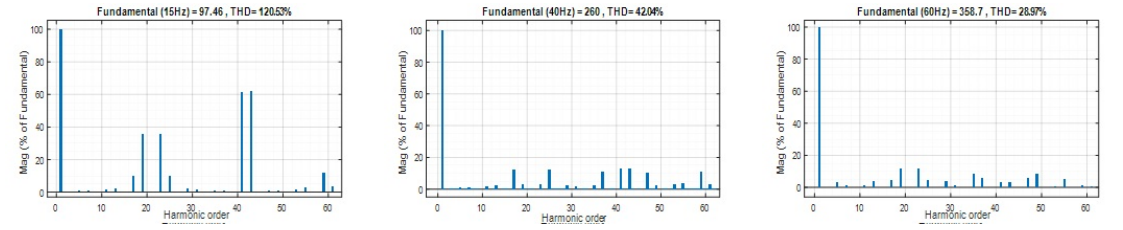

(d) For m_a=0.3 (e) For m_a=0.8 (f) For m_a=1.2

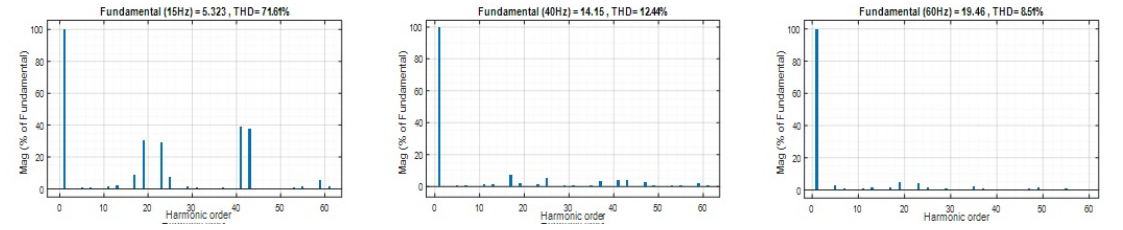

(g) For m_a=0.3 (h) For m_a=0.8 (i) For m_a=1.2

Fig. 4.4: Simulation results of the cascaded three-level inverter obtained with SPWM showing the output voltages ((a), (b) and (c)), phase voltage THD ((d), (e) and (f)) and Phase current THD ((g), (h) and (i)) for m_a = 0.3, 0.8 and 1.2 respectively

generate the similar fundamental voltage at lower modulation indices but at higher modulation index, CO-SFO-PWM has a considerable drop in fundamental voltage magnitude as seen from Figs. 4.4(e), 4.5(e) and 4.6(e) while SFO-PWM and SPWM generates a similar value of the fundamental voltage. Stepping further into overmodulation region as shown in Figs. 4.4(f), 4.5(f) and 4.6(f), SFO-PWM becomes superior over the other two PWMs as the peak of the modified modulating waveform reduces due to the addition of a third harmonic component. So, even upto some extent in over modulation the modified modulated sine wave peak stays below the carrier peak and continues its linearity. The output fundamental saturates only when the modulation wave peak crosses the carrier peak.

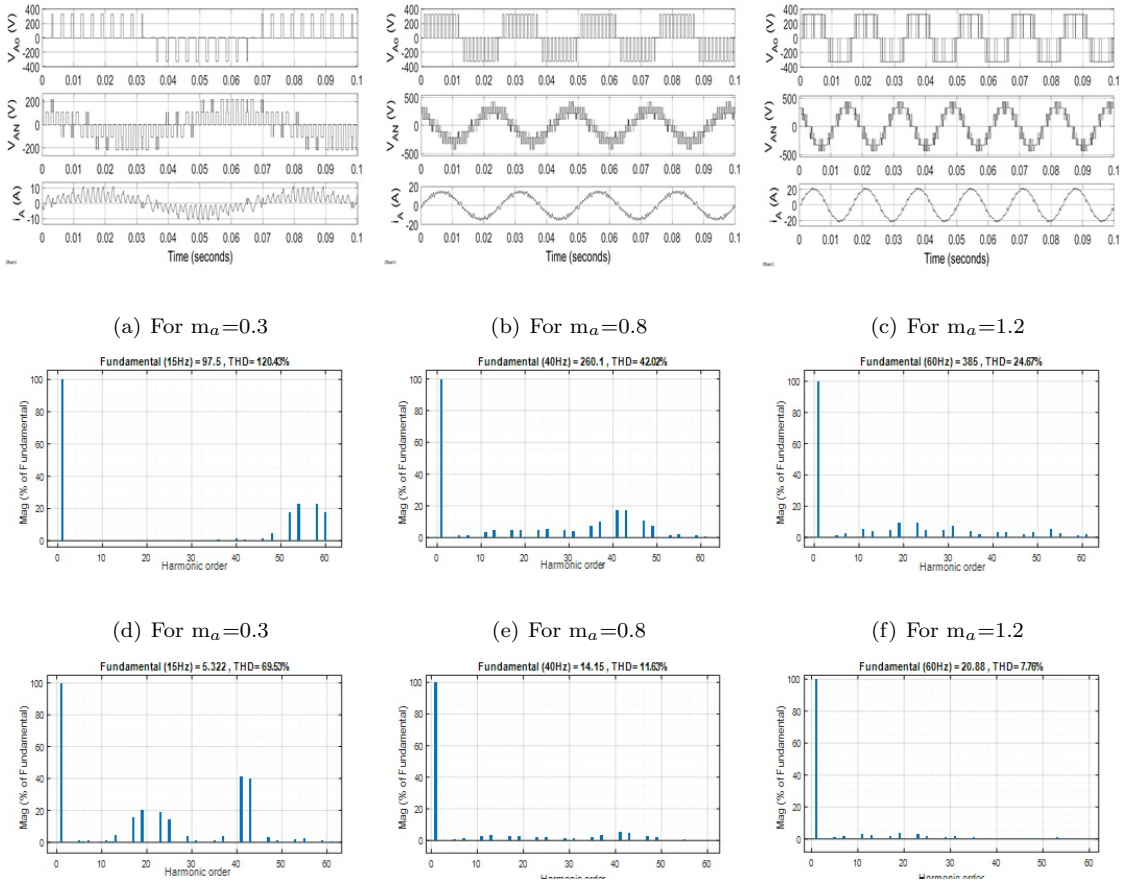

(a) For m_a=0.3 (b) For m_a=0.8 (c) For m_a=1.2

(d) For m_a=0.3 (e) For m_a=0.8 (f) For m_a=1.2

(g) For m_a=0.3 (h) For m_a=0.8 (i) For m_a=1.2

Fig. 4.5: Simulation results of the cascaded three-level inverter obtained with SFO-PWM showing the output voltages ((a), (b) and (c)), phase voltage THD ((d), (e) and (f)) and Phase current THD ((g), (h) and (i)) for m_a = 0.3, 0.8 and 1.2 respectively

From the above discussion it is clear that at lower m_a values CO-SFO-PWM stands out among the three PWMs with reduced THD in phase voltage and current and at higher m_a values, SFO-PWM has better fundamental voltage magnitudes. Therefore, plotting of THDs and fundamental voltage magnitudes against more number of m_a values, will give a better understanding. So, best two PWMs among the three, relative to each of lower and higher modulation ranges are compared below.

SPWM and SFO-PWM are best among the three at higher modulation indices as discussed above. It can be seen from the voltage THDs plot in Fig. 4.7, both the SPWM and SFO-PWM have almost similar characteristics, except that SFO-PWM has slight improved THD in overmod-

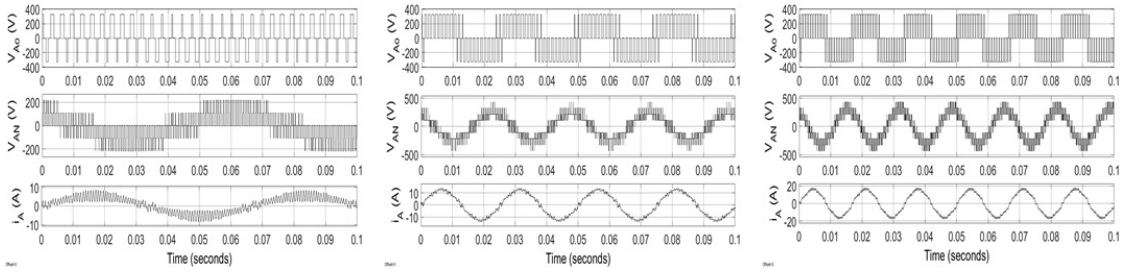

(a) For m_a=0.3 (b) For m_a=0.8 (c) For m_a=1.2

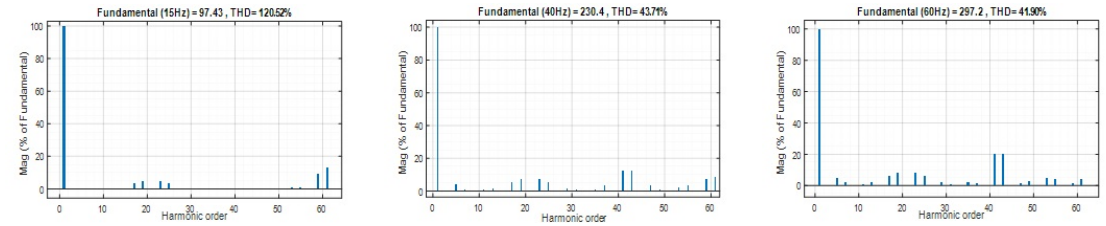

(d) For m_a=0.3 (e) For m_a=0.8 (f) For m_a=1.2

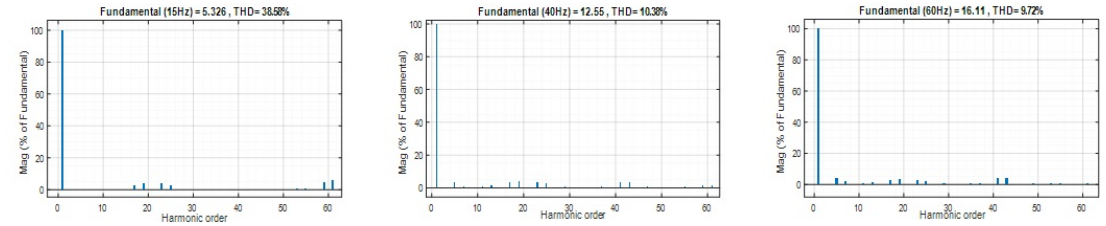

(g) For m_a=0.3 (h) For m_a=0.8 (i) For m_a=1.2

Fig. 4.6: Simulation results of the cascaded three-level inverter obtained with CO-SFO-PWM showing the output voltages ((a), (b) and (c)), phase voltage THD ((d), (e) and (f)) and Phase current THD ((g), (h) and (i)) for m_a = 0.3, 0.8 and 1.2 respectively

ulation region. It can be seen from Fig. 4.8 i.e fundamental output voltage magnitude variation w.r.t m_a, the SFO-PWM has higher fundamental magnitude in overmodulation region as mentioned earlier. Such a behaviour is good for certain applications, where faster acceleration and quick speed response of motor is required, motor can be driven with overmodulation for a short span of time instead of going for a higher DC bus value.

For lower modulation ranges, SFO-PWM and CO-SFO-PWM provides lower THDs than SPWM and the output current THD obtained with the is plotted against m_a values and is shown in Fig. 4.9. It can be seen from Fig. 4.9 that the CO-SFO-PWM method has this reduced phase

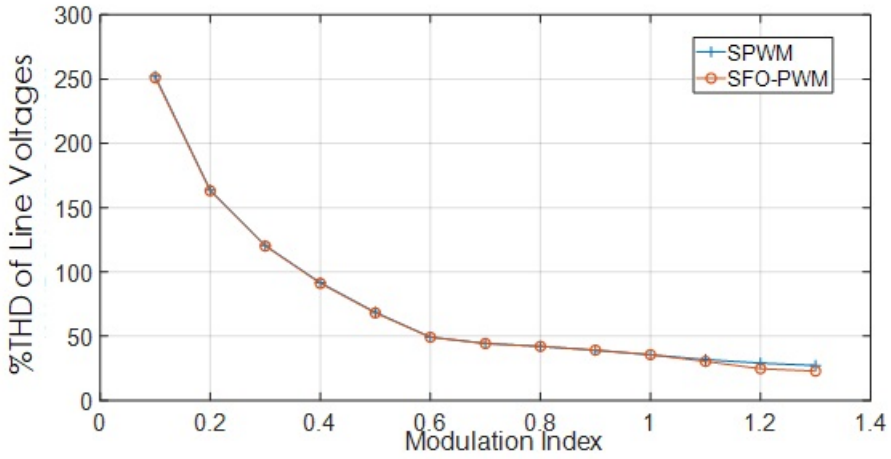

Fig. 4.7: Voltage THD plotted against Modulation index for SPWM and SFO-PWM

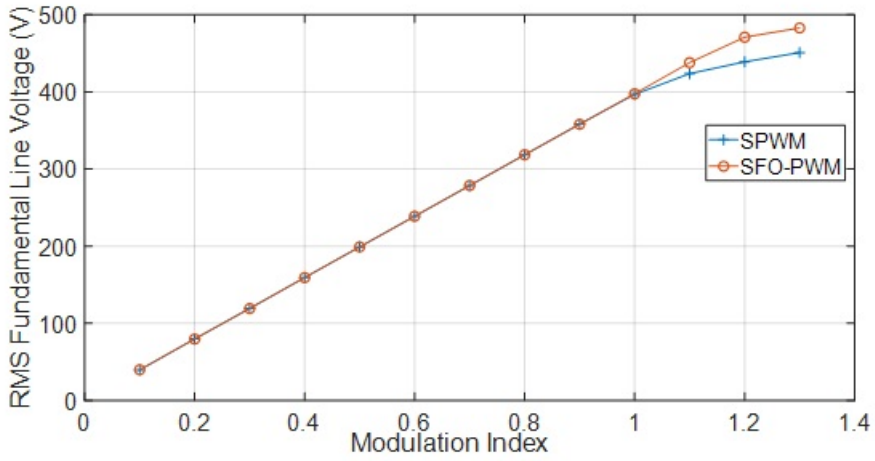

Fig. 4.8: Fundamental RMS voltage plotted against Modulation index for SPWM and SFO-PWM

current THDs continued upto m_a=0.8 and then merged with SFO-PWM. Comparing the fundamental voltage magnitude variation w.r.t m_a as shown in Fig. 4.10, the plot of CO-SFO-PWM deviates towards reduced voltages early at m_a=0.6 and this limits the benefits of CO-SFO-PWM only upto lower m_a values, whereas SFO-PWM is good for higher m_a values. Hence, there is a need for a hybrid PWM method that ensures the benefits of both CO-SFO-PWM and SFO-PWM in entire modulation range.

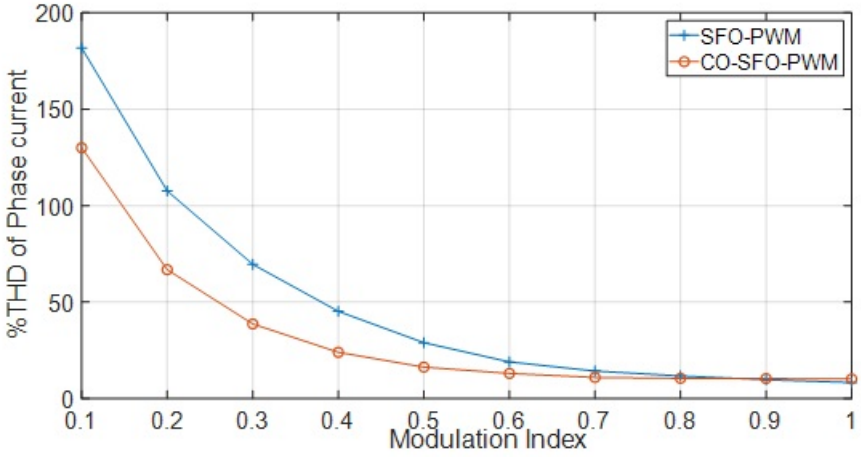

Fig. 4.9: Current THD plotted against Modulation index for SFO-PWM and CO-SFO-PWM

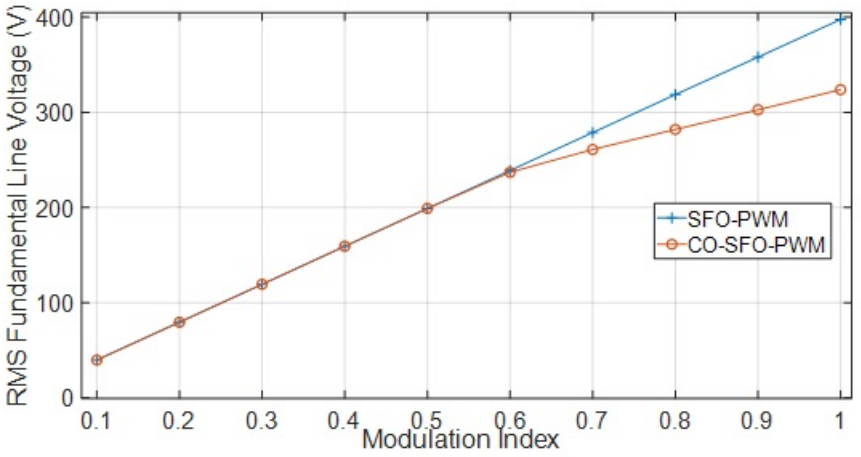

Fig. 4.10: Fundamental RMS voltage plotted against Modulation index for SFO-PWM and CO-SFO-PWM

4.2.1 Hybrid Switchover PWM method

Operating with CO-SFO-PWM under lower modulation indices and a direct switching over to SFO-PWM at an m_a of 0.56 is reported in [10]. But with such a sudden switch over, the reduced THD benefits of CO-SFO-PWM extended till m_a=0.8, will be lost. Instead of such sudden switching, if a soft transition of PWMs with a gradual change of carrier overlap region can reap more benefits. This gradual change of overlap region can be made in different ways, under different ranges of m_a as shown in Fig. 4.11. An m_a range of 0.4 to 0.8 is chosen to PWM

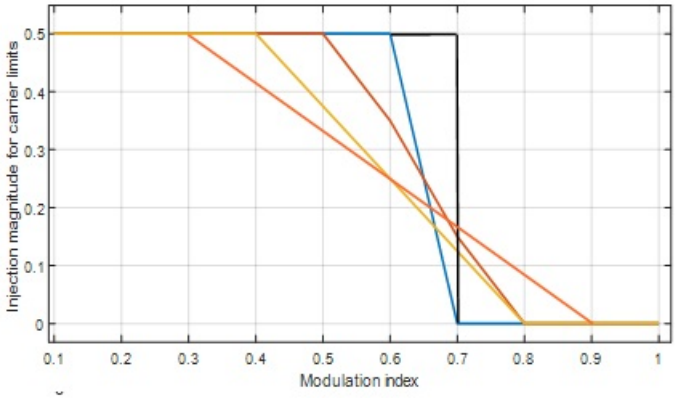

Fig. 4.11: Different ranges of m_a for switching over of PWMs

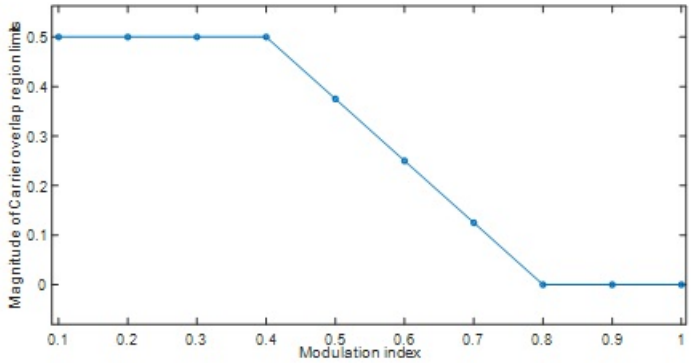

Fig. 4.12: Hybrid PWM transition in 0.4 to 0.8 m_a range

transition, for covering the maximum best points from both the PWMs from the plots shown in Figs. 4.9, 4.10.

The magnitude of the carrier overlap with the modulation index in the proposed hybrid PWM is shown in Fig. 4.12 and the corresponding carrier waveforms with the proposed hybrid PWM are shown in Fig. 4.13. In Fig. 4.13, we can clearly observe that the overlap region starts gradually decreasing from m_a=0.4 and reaches zero at m_a=0.8. To highlight the benefits of this gradual change in the overlap with this choice of m_a values, the fundamental voltage magnitude and phase current THD with all the three PWMs are plotted w.r.t m_a values and are presented in Figs. 4.14 and 4.15 respectively. It can be seen from Fig. 4.14, the proposed hybrid PWM gives most of the higher voltage values from both the CO-SFO-PWM and SFO-PWM. It can be seen from Fig. 4.15, the proposed hybrid PWM method has completely captured the reduced THD benefits of

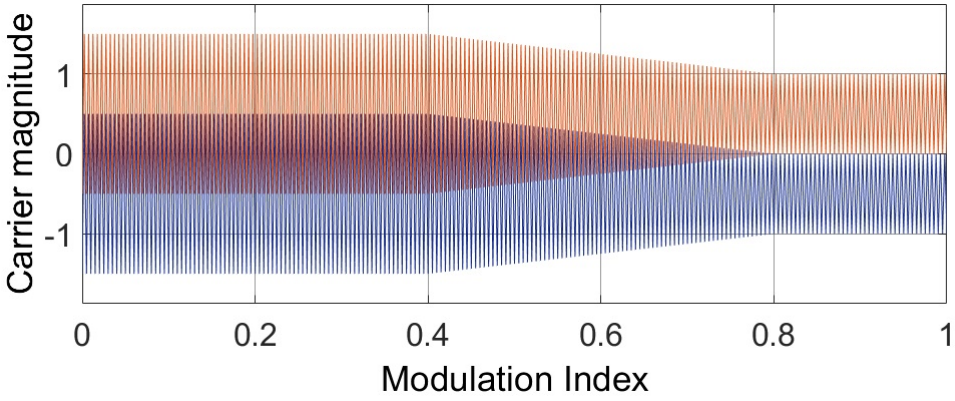

Fig. 4.13: Variation of overlap region as modulation increases from 0 to 1 from left to right of x-axis

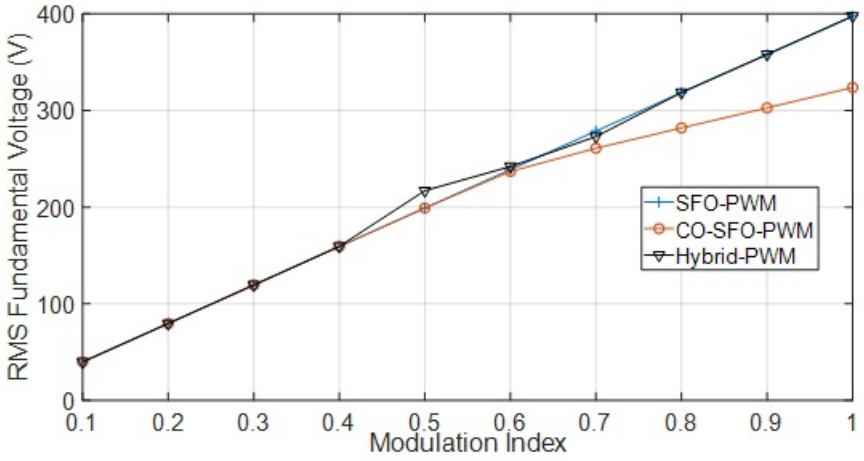

Fig. 4.14: Fundamental RMS voltage plotted against Modulation index for SFO-PWM, CO-SFO-PWM and Hybrid-SO-PWM

CO-SFO-PWM for full range of m_a. Hence, the use of the proposed hybrid PWM for a motor drive provides reduced THD over wide range of speed without a requirement for an increase in the DC bus voltage.

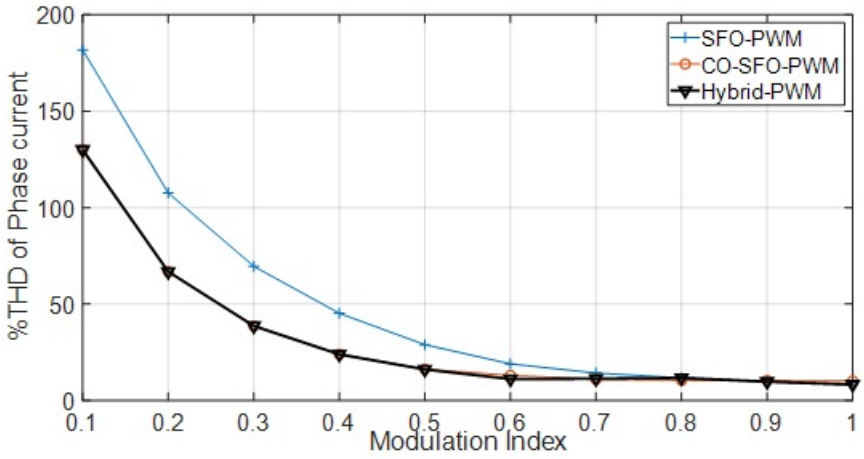

Fig. 4.15: Current THD plotted against Modulation index for SFO-PWM and CO-SFO-PWM and Hybrid-SO-PWM

4.3 FOC with hybird PWM for cascaded three-level inverter fed induction motor drive

The FOC with the proposed hybrid PWM is implemented on the three-level cascaded inverter fed induction motor drive and the dynamic and steady state results obtained are presented in detail in this section. Using the block diagram of overall control system as shown in Fig. 2.8, a simulation model is developed in MATLAB as shown in Fig.4.16 which shows the power circuit of the cascaded inverter fed induction motor in Fig. 4.16(a) and the control system implementation part shown in Fig. 4.16(b). The parameters of the induction motor are given in Table 2.1.

Table 4.1: PI controller gain constant values

PI CONTROLLER LOOP POSITION	K_p VALUE	K_i VALUE
d-axis Current Loop	70.25	3437.12
q-axis Current Loop	168.6	12029.92
Rotor Flux Loop	580.72	45.5015
Rotor Speed Loop	36	0.068

The gain constants obtained in section 2.2 of chapter 2 are taken as the starting values to

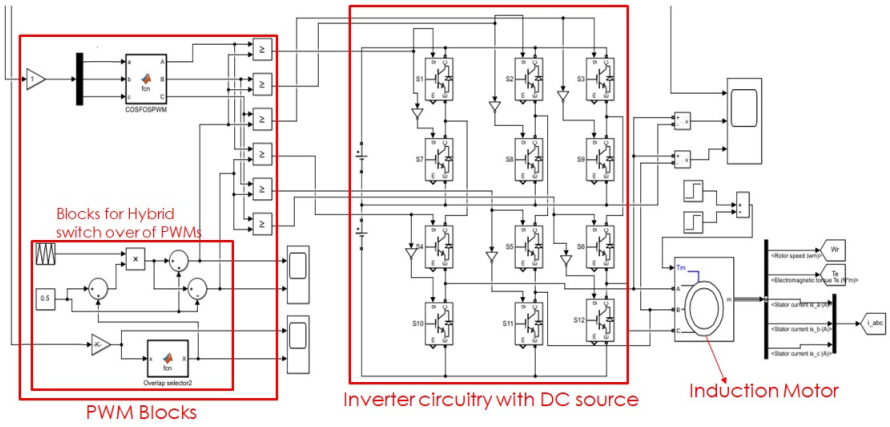

(a) Power Circuit part of the simulation model

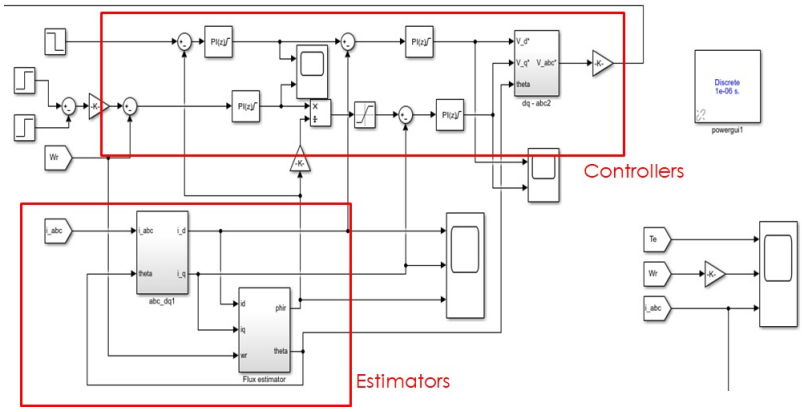

(b) Control system part of the simulation model

Fig. 4.16: Simulation model for FOC of Cascaded three-level inverter fed induction motor drive developed in MATLAB

implement the simulation and require further tuning to produce fast and smooth responses. The further tuning of these parameters is done by thoughtfully changing the values in multiples of the starting values in a trial and error manner to get the final set of controller gains and the final values of the controller gains are given in Table 4.3. The saturation limits at each PI controller is set to the calculated rated parameters as per Table 2.2 with an exception in the torque limits. The torque limits are set at a value equal to 1.25 times the rated motor torque which facilitates the motor to accelerate and decelerate faster and thus providing a good dynamic response of the system. The simulation model is subjected to variations in the speed command and the load torque and the corresponding responses obtained for the dynamic changes are presented in detail.

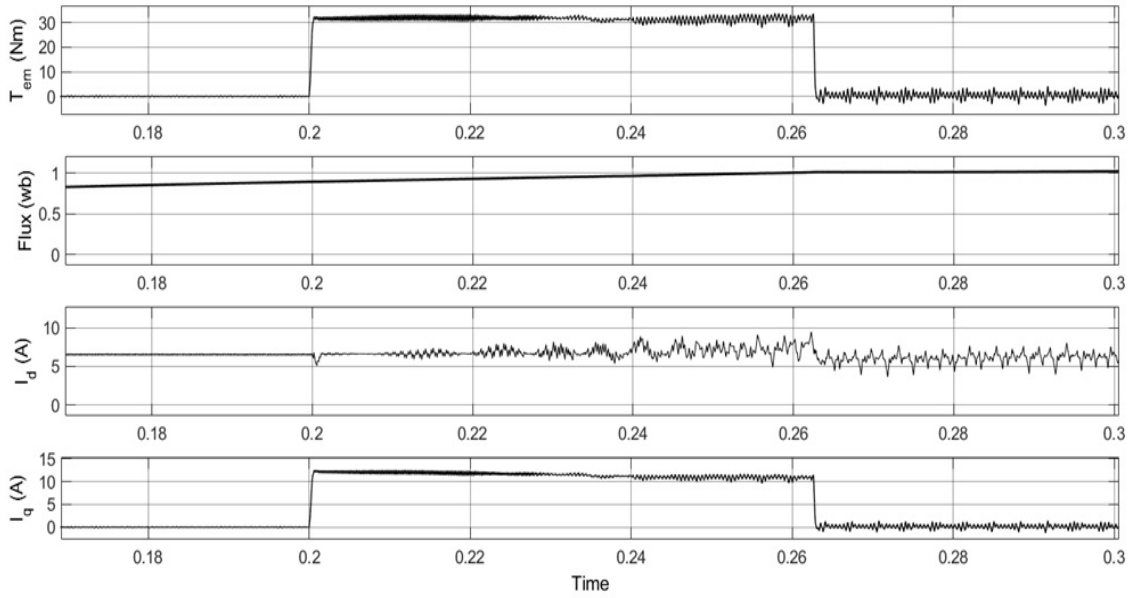

Figure 4.17: T, ϕ, i_d, i_q responses during staring of the drive

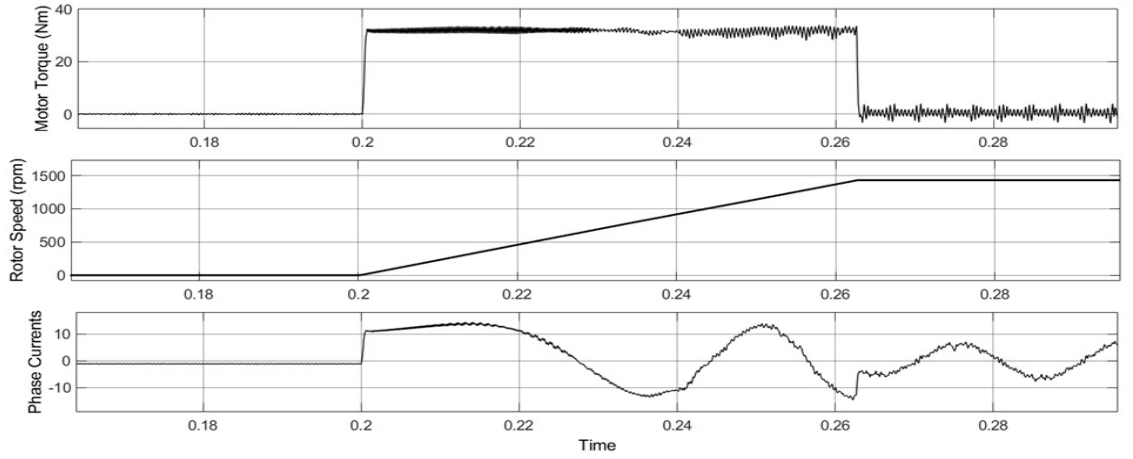

Figure 4.18: T, speed, i_a responses during staring of the drive

Firstly, starting response of the motor drive is presented. For this, the reference speed command is increased from from zero to its rated value at t = 0.2 s and the response of the drive showing the Torque, flux and the d-q components of the stator currents is shown in Fig. 4.17. The corresponding speed and the phase current of the motor during starting are given in Fig. 4.18. It can be observed from Figs. 4.17 and 4.18 that the machine torque quickly raised to the limit set in the control (1.25 times rated torque) so as to allow the acceleration of the motor and the motor speed smoothly increases and reaches the reference value in about 0.07 secs. Once the speed reaches the rated value the torque reduces to zero. The value of I_d is held almost constant during

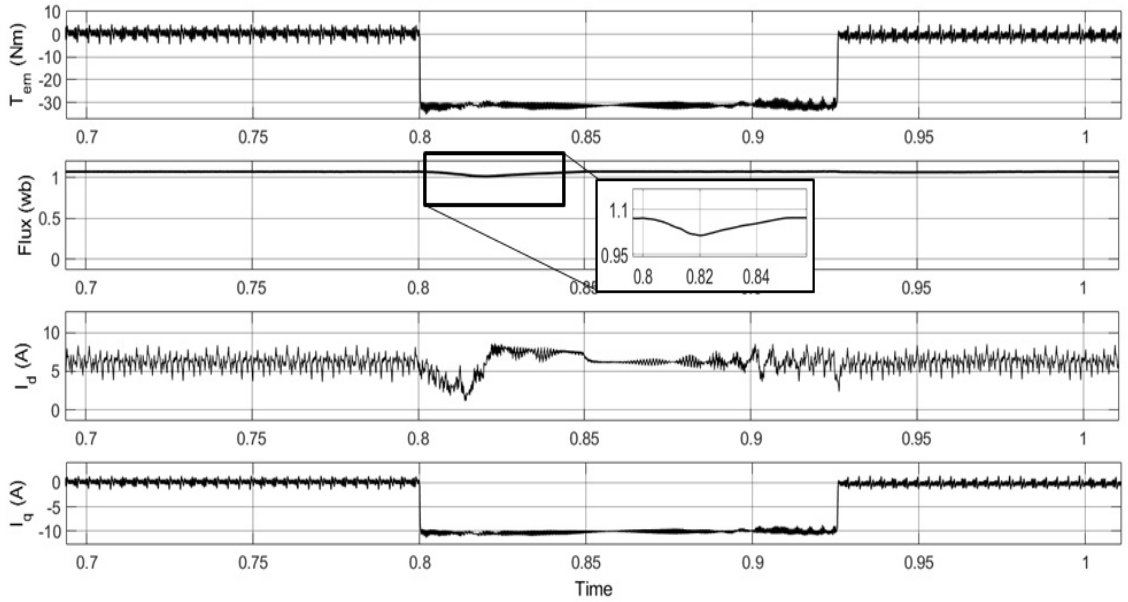

Fig. 4.19: T, ϕ, i_d, i_q responses during speed reversal

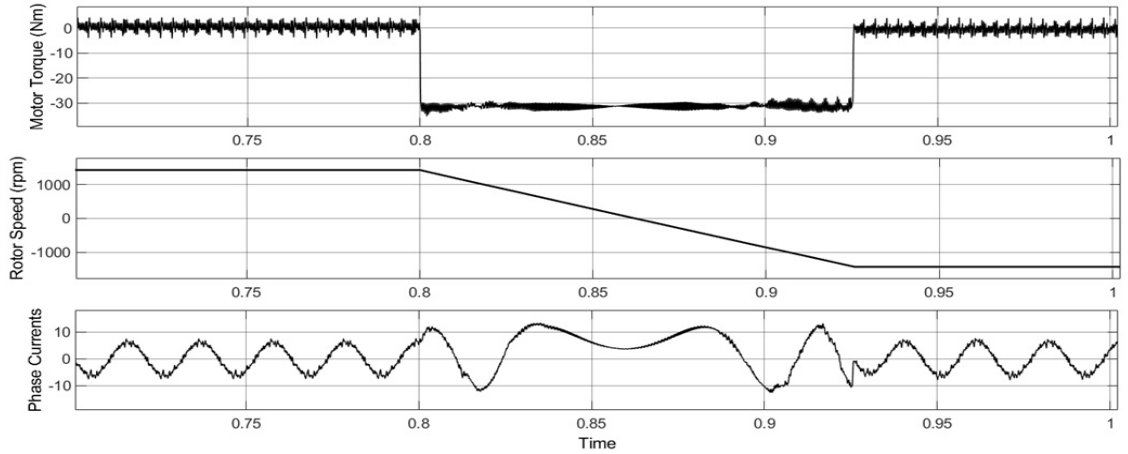

Fig. 4.20: ϕ, T, speed, i_a responses during speed reversal

the staring process indicating that the rotor flux is constant, while the I_q waveform follows the torque as both I_q and Torque are proportional under rotor field orientation and this clearly shows the independent control of torque and flux offered by FOC. For considerable changes in torque magnitude, dip in i_d is observed in Fig. 4.21, but it readily averages to the steady state value due to PI controlling action.

Next, the drive is tested for speed reversal from rated speed. For this, the reference speed of

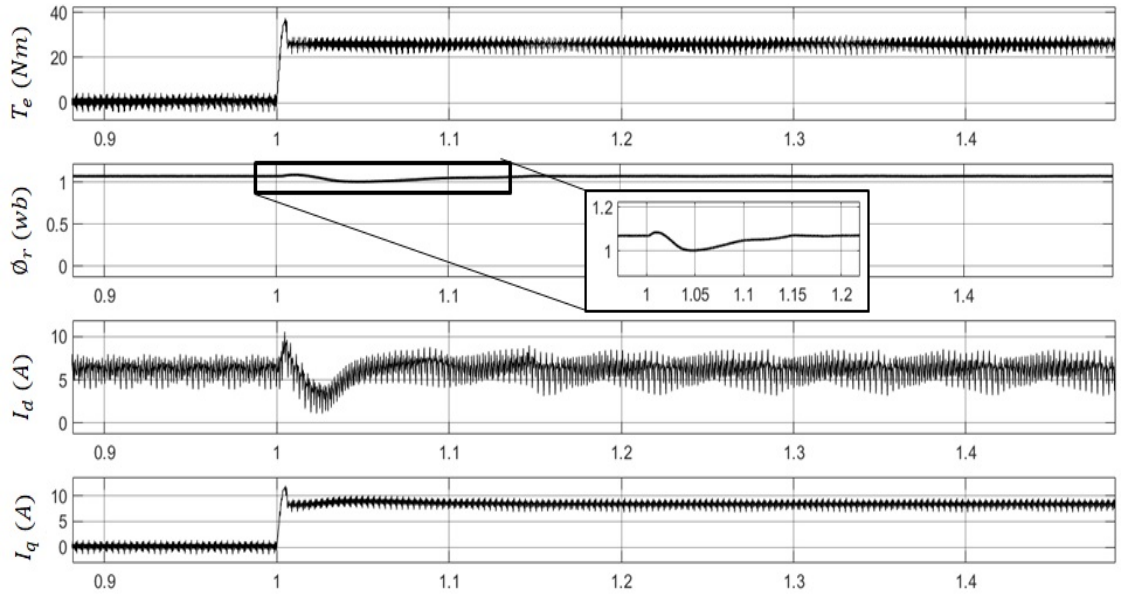

Fig. 4.21: T, ϕ, i_d, i_q responses for rated loading conditions

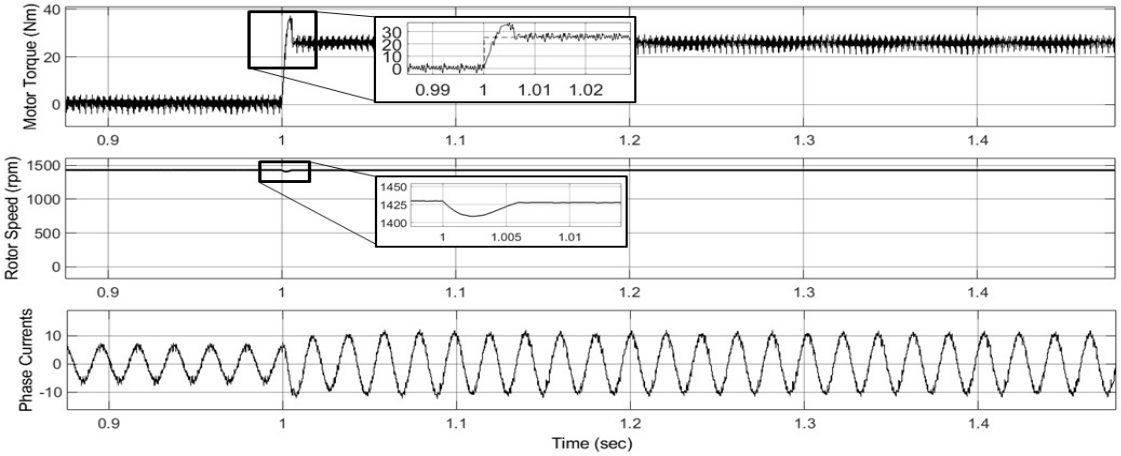

Fig. 4.22: ϕ, T, speed, i_a responses for rated loading conditions

the motor is changed from +1430rpm to -1430rpm and the results obtained showing the torque, speed, flux and the stator current are shown in Figs. 4.19 and 4.20. It can be observed from the Fig. 4.19, a small drop in flux for the negative change of torque when speed reversal command is initiated and the same is noticed with i_d response also, but immediately pulled up to the rated value. The motor torque quickly reaches the limiting value of -1.25T_{rated} to allow the deceleration of the motor and remains at that value until the motor speed smoothly reaches to the reference

value of -1430 rpm. It can be seen from Fig. 4.20, the stator current phase reversal during the speed reversal is proper and no overshoots in the stator current are observed.

Lastly, the drive is subjected to a load test. To perform this test, initially the motor is made to run at the rated speed and suddenly a step change in the load torque equal to the rated torque of 26 Nm is given at t = 1 s and the results showing the motor torque, flux, speed and the stator current are shown in Figs. 4.21 and 4.22. It can be seen from Fig. 4.21 that there is the motor torque increases to meet the load torque and as the value of i_q increases momentarily keeping i_d constant, a small overshoot in the flux is observed and this is immediately corrected by the i_d control loop. It can also be seen from Figs. 4.21 and 4.22, that due to the sudden loading, a small dip in the motor speed can be observed which is immediately corrected with a small overshoot in the torque. This is clearly shown in the zoomed in portion of the Fig. 4.22.

From the results, we can infer that the closed loop rotor field orientation FOC method is facilitating the system to withstand stably for any kind of loading disturbances. CO-SFO-PWM gives less ripple content in currents and torques at no load conditions which extends for light load conditions. While the SFO-PWM gives a better dynamic response when machine is operating around the rated conditions. Incorporating both PWMs, the Hybrid PWM transition method proposed in this thesis significantly reduces ripple content in output phase currents, offering reduced losses and better efficiency of operation, without compromising the available rated speed range for operation.

Chapter 5

Conclusion

This thesis presents a FOC scheme based closed loop control of IM drive. The indirect rotor FOC for the induction motor drive greatly simplifies the dynamic d-q model of the motor reduces the control complexity to facilitate the independent control over torque and flux.

The cascaded three-level inverter requires lesser number of power semiconductor devices and isolated DC power supplies, compared with other traditional three-level inverter topologies. It is shown from the results that the cascaded three-level inverter fed induction motor drive gives superior performance in terms of reduced torque ripple when compared to that of two-level inverter and gives almost the same performance compared to a three-level NPC inverter. However, unlike the three-level NPC inverter, this inverter model is free from neutral point voltage fluctuations.

The carrier based PWMs are simple in implementation when compared with the conventional space vector based PWM and selective harmonic PWM methods. From the carrier based PWMs implementations for cascaded three-level inverter, the CO-SFO-PWM and SFO-PWM presented in this work has given superior performance at lower and higher modulation indices respectively when compared to conventional sinusoidal PWM. A hybrid PWM using CO-SFO-PWM and SFO-PWM with a smooth transition is implemented to reduce the overall harmonic content in the motor current and enables to efficiently utilize the entire speed range of the motor. From the PWM simulation results obtained for the cascaded three-level inverter connected to an RL-load, we observed that the hybrid transition of PWMs is producing reduced THDs within the entire

modulation range when compared with any one PWM being operated alone.

Simulating for the operation of entire closed loop, results are obtained for speed reversal and torque change commands and found to be satisfactory. The FOC method along with cascaded three-level inverter has produced a better torque dynamic response for all kinds of disturbances created, within the ratings. The hybrid PWM method inhabiting CO-SFO-PWM at lower speeds and SFO-PWM at higher speeds, has shown its suitability, reliability and stability for entire speed range with reduced current harmonics.

REFERENCES

[1] Modern Power Electronics by Bimal K.Bose,Published by Prentice Hall, Year-2002, Pages: 333-435.

[2] Electric Motor Drives- Modelling, Analysis and Control by R,Krishnan,Published by Prentice Hall, Year-2001, Pages: 196-220 & 411-511.

[3] Analysis of Electric Machinery and Drive System by Paul C. Krause, Oleg Wasynczuk and Scott D. Sudhoff, Second edition, IEEE Power Engineering Society sponsored, IEEE Press, Year- 2022, Pages: 109-185 and 525-554.

[4] Naga Surya Prakash M and S. Srinivas, "Field Oriented Control of an Open End Winding Induction Machine with zero Common Mode Voltage," National Power Electronics Conference (NPEC), Dec 18-20, 2017.

[5] Hridaya I and S. Srinivas, "Direct Torque Control of a Cascaded Three Level inverter driven Induction Motor", IEEE Conference on Power Electronics, Drives and Energy Systems (PEDES), 2014.

[6] A. Nabae, K. Otsuka, H. Uchino and R. Kurosawa, "An Approach to Flux Control of Induction Motors Operated with Variable-Frequency Power Supply," in IEEE Transactions on Industry Applications, vol. IA-16, no. 3, pp. 342-350, May 1980.

[7] D. Casadei, F. Profumo, G. Serra and A. Tani, "FOC and DTC: two viable schemes for induction motors torque control," in IEEE Transactions on Power Electronics, vol. 17, no. 5, pp. 779-787, Sep 2002.

[8] H. Stemmler and P. Guggenbach, "Configurations of high-power voltage source inverter drives," 1993 Fifth European Conference on Power Electronics and Applications, Brighton, UK, 1993, pp. 7-14 vol.5.

[9] H. Abu-Rub, J. Holtz, J. Rodriguez and G. Baoming, "Medium-Voltage Multilevel ConvertersState of the Art, Challenges, and Requirements in Industrial Applications," in IEEE Transactions on Industrial Electronics, vol. 57, no. 8, pp. 2581-2596, Aug. 2010.

[10] Pratibha Naganathan and Srirama Srinivas, "Hybrid PWM Methods for Harmonic Reduction in Neutral Point Clamped Three-Level Inverter Drive for Pump Applications", Electric Power Components and Systems, 48(14-15): 1474–1487, 2021 Taylor & Francis Group, LLC.

[11] Hridaya I and S. Srinivas, "Carrier Overlapped PWM Switching Schemes for a Cascaded Three Level Voltage Source Inverter", IEEE International Conference on Industrial Technology (ICIT), 2015.

[12] D. G. Holmes and T. A. Lipo, "Pulse Width Modulation for Power Converters: Principles and Practice". Hoboken, USA: John Wiley Sons, 2003, vol. 18.

[13] C. I. Odeh, "Balancing switching losses in three-phase, fivelevel pulse-width modulation switched voltage source inverter using hybrid modulation techniques," Electric Power Components Syst., vol. 42, no. 11, pp. 1194–1200, 2014.

[14] T. A. Lipo and Q. Jiang, "Switching angles and dc link voltages optimization for multilevel cascade inverters," Electric Machines Power syst., vol. 28, no. 7, pp. 605–612, 2000.

[15] B. Chokkalingham, S. Padmanaban, and F. Blaabjerg, "Investigation and comparative analysis of advanced pwm techniques for three-phase three-level npc-mli drives," Electric Power Components Syst., vol. 46, no. 3, pp. 258–269, 2018.

[16] T. H. Abdelhamid and K. M. El-Naggar, "Optimal pwm control of a new generalized family of multilevel inverters," Electric Power Components Syst., vol. 36, no. 1, pp. 73–92, 2007.

[17] S. K. Sahoo and T. Bhattacharya, "Phase-shifted carrierbased synchronized sinusoidal pwm techniques for a cascaded h-bridge multilevel inverter," IEEE Trans. Power Electron, vol. 33, no. 1, pp. 513–524, Jan 2018.

[18] Q. Huang and A. Q. Huang, "Feedforward proportional carrier- based pwm for cascaded h-bridge pv inverter," IEEE J. Emerg. Sel. Topics Power Electron, vol. 6, no. 4, pp. 2192–2205, Dec 2018.

[19] P. Naganathan and S. Srinivas, "Spectral analysis of spwm controlled cascaded three-level inverter drive," 2016 IEEE Region 10 Conference (TENCON), 2016. in Nov pp. 697–702.

[20] H. Wang, R. Zhao, Y. Deng, and X. He, "Novel carrierbased pwm methods for multilevel inverter," in IECON'03. 29th Annual Conference of the IEEE Industrial Electronics Society (IEEE Cat. No.03CH37468), vol. 3, Nov, 2003., pp. 2777–2782 Vol.3.

[21] G. Carrara, S. Gardella, M. Marchesoni, R. Salutari, and G. Sciutto, "A new multilevel PWM method: a theoretical analysis," IEEE Trans. Power Electron., vol. 7, no. 3, pp. 497–505, Jul 1992.